Tundra wildfire triggers sustained lateral nutrient loss in Alaskan Arctic

Benjamin W. Abbott[1], Adrian V. Rocha[2], Arial Shogren[3], Jay P. Zarnetske[3], Frances Iannucci[4,5], William B. Bowden[4], Samuel P. Bratsman[1], Leika Patch[1], Rachel Watts[1], Randy Fulweber[6], Rebecca J. Frei[1,7], Amanda M. Huebner[1], Sarah M. Ludwig[8], Gregory T. Carling[9], Jonathan A. O'Donnell[10]

[1]Brigham Young University, Department of Plant and Wildlife Sciences, Provo, Utah, USA

[2]University of Notre Dame, Department of Biological Sciences & the Environmental Change Initiative, Notre Dame, Indiana, USA

[3]Department of Earth and Environmental Sciences, Michigan State University, East Lansing, Michigan, USA

[4]University of Vermont, Rubenstein School of Environment and Natural Resources, Burlington, Vermont, USA

[5]University of Alaska Fairbanks, Department of Biology and Wildlife, Fairbanks, Alaska, USA

[6]University of Alaska Fairbanks, Toolik GIS, Fairbanks, Alaska, USA

[7]University of Alberta, Department of Renewable Resources, Edmonton, Alberta, Canada

[8]Columbia University, Department of Earth and Environmental Science, NY, New York

[9]Brigham Young University, Department of Geological Sciences, Provo, Utah, USA

[10]Arctic Network, National Park Service, Anchorage, AK 99501, USA

Running head: Lateral nutrient loss after tundra wildfire

Key words: Tundra, Wildfire, Nutrient flux, Streams, Permafrost, Arctic, Watershed, Ecosystem succession, Hydrology, Disturbance

Abstract: Climate change is creating widespread ecosystem disturbance across the permafrost zone, including a rapid increase in the extent and severity of tundra wildfire. The expansion of this previously rare disturbance has unknown consequences for lateral nutrient flux from terrestrial to aquatic environments. Lateral loss of nutrients could reduce carbon uptake and slow recovery of already nutrient-limited tundra ecosystems. To investigate the effects of tundra wildfire on lateral nutrient export, we analyzed water chemistry in and around the 10-year-old Anaktuvuk River fire scar in northern Alaska. We collected water samples from 21 burned and 21 unburned watersheds during snowmelt, at peak growing season, and after plant senescence in 2017 and 2018. After a decade of ecosystem recovery, aboveground biomass had recovered in burned watersheds, but overall carbon and nitrogen remained ~20% lower, and the active layer remained ~10% deeper. Despite lower organic matter stocks, dissolved organic nutrients were substantially elevated in burned watersheds, with higher flow-weighted concentrations of organic

carbon (25% higher), organic nitrogen (59% higher), organic phosphorus (65% higher), and organic sulfur (47% higher). Geochemical proxies indicated greater interaction with mineral soils in watersheds with surface subsidence, but optical analysis and isotopes suggested that recent plant growth, not mineral soil, was the main source of organic nutrients in burned watersheds. Burned and unburned watersheds had similar $\delta^{15}N\text{-}NO_3^-$, indicating that exported nitrogen was of pre-burn origin (i.e. not recently fixed). Lateral nitrogen flux from burned watersheds was 2- to 10-fold higher than rates of background nitrogen fixation and atmospheric deposition estimated in this area. These findings indicate that wildfire in Arctic tundra can destabilize nitrogen, phosphorus, and sulfur previously stored in permafrost via plant uptake and leaching. This plant-mediated nutrient loss could exacerbate terrestrial nutrient limitation after disturbance or serve as an important nutrient release mechanism during succession.

Introduction

Climate change is triggering widespread ecosystem disturbance across the permafrost zone (Mack *et al* 2011, Abbott *et al* 2016b, Biskaborn *et al* 2019). Wildfire and permafrost degradation, which are the most common disturbance types in Boreal and Arctic ecosystems, respectively (Bond-Lamberty *et al* 2007, Jones *et al* 2015, Kim *et al* 2020, Kokelj and Jorgenson 2013), can mobilize organic matter and inorganic nutrients previously protected by cold and wet conditions (Balshi *et al* 2009, Abbott *et al* 2015, Walker *et al* 2019, Rodríguez-Cardona *et al* 2020). Whether nutrients liberated from thawing permafrost are available to terrestrial and aquatic primary producers will regulate key components of the Arctic carbon cycle and energy balance, including: the magnitude of carbon dioxide (CO_2) fertilization effects on net primary productivity (McGuire *et al* 2018, Balshi *et al* 2009); the rate and type of ecosystem recovery following disturbance (Kou *et al* 2020, Pearce *et al* 2014, Chen *et al* 2018); the stability of soil organic matter (Mack *et al* 2004, Craine *et al* 2007); shifts in vegetation (Mack *et al* 2008, Pearce *et al* 2014, Jiang *et al* 2015a); aquatic and marine primary productivity (Carey *et al* 2019, McClelland *et al* 2014, Creed *et al* 2018, Wologo *et al* 2020); and surface energy balance (Rocha and Shaver 2011b, Loranty *et al* 2018). Consequently, potential changes in nutrient availability are a major source of uncertainty in predicting net ecosystem carbon balance of the permafrost zone (McGuire *et al* 2018, Jiang *et al* 2015b, Hoffman *et al* 2017, Jiang *et al* 2017, Shogren *et al* 2020, Wright and Rocha 2018).

Wildfire is already common in forest and some tundra ecosystems, where it structures the above and belowground carbon stocks and vegetation community (Balshi *et al* 2009, Rocha and Shaver 2011a, Racine *et al* 2004, Jones *et al* 2013, Kim *et al* 2020). In Arctic tundra, wildfire is projected to increase 4- to 11-fold by 2100 due to increased temperature, evapotranspiration, ignition sources, and vegetation shifts (Abbott *et al* 2016b, Hu *et al* 2010, 2015). Because wildfire has been relatively rare in Arctic tundra in the past (Higuera *et al* 2011, Rocha *et al* 2012, Jones *et al* 2013), it remains uncertain how changes in this key ecosystem disturbance will affect vertical (land-atmosphere) and lateral (land-water) nutrient fluxes (Larouche *et al* 2015, Parham *et al* 2013, Rodríguez-Cardona *et al* 2020, Voigt *et al* 2020, Ludwig *et al* 2018).

Increased tundra wildfire could affect nutrient dynamics in several interrelated ways, depending on the timing and location of changes in nutrient supply and demand (Fig. 1). On the supply side, wildfire can remove a substantial proportion of aboveground and belowground nutrients via combustion (Mack *et al* 2011, Bret-Harte *et al* 2013), decreasing organic nutrient sources and potentially lateral nutrient flux immediately postfire (Betts and Jones 2009, Kawahigashi *et al* 2011, Rodríguez-Cardona *et al* 2020, Parham *et al* 2013). However, the combustion of surface vegetation and peat decreases insulation and albedo, enhancing heat transfer into soils and deepening the seasonally-thawed active layer (Loranty *et al* 2018, Hu *et al* 2015, Jiang *et al* 2014, Jones *et al* 2015, Holloway *et al* 2020). This can allow water to flow through deeper soil horizons, which are often richer in solutes and inorganic nutrients, increasing nutrient supply (Hewitt *et al* 2015, Salmon *et al* 2018, Frey and McClelland 2009, Kawahigashi *et al* 2011). In areas of ice-rich permafrost, active-layer thickening can trigger permafrost collapse and thermal erosion, known as thermokarst (Jones *et al* 2015, Larouche *et al* 2015, Kokelj and Jorgenson 2013). Thermokarst releases above and belowground nutrients abruptly, temporarily increasing aquatic nutrient availability while decreasing terrestrial stocks (Turetsky *et al* 2019, Abbott *et al* 2015, Vonk *et al* 2015, Harms *et al* 2014, Buckeridge *et al* 2016, Abbott and Jones 2015). On the demand side, the combustion of vegetation could initially decrease terrestrial nutrient demand, followed by increased uptake during vegetation regrowth (Carey *et al* 2019, Malone *et al* 2018, Bret-Harte *et al* 2013). Wildfire could also create temporal mismatches in nutrient supply and demand. For example, a deeper active layer or the development of taliks (layers of unfrozen soil beneath the active layer), which can be triggered by wildfire (Viereck *et al* 2008, Yoshikawa *et al* 2002), allows flow to persist through a longer portion of the year,

including after the end of the growing season when terrestrial nutrient demand decreases (Treat *et al* 2016, Larouche *et al* 2015, Shogren *et al* 2020, Buckeridge and Grogan 2010, Rey *et al* 2020).

Finally, changes in vegetation driven by climate and disturbance could alter the timing and amount of terrestrial nutrient uptake and release. The stature and composition of plant communities is rapidly changing in high-latitude catchments (Walker *et al* 2006, Myers-Smith *et al* 2015, Sturm *et al* 2001, Carey *et al* 2019), and shifting plant communities could either increase or decrease lateral nutrient loss depending on the emerging community's nutrient acquisition strategies, such as nitrogen fixation, mycorrhizal association, and rooting depth (Rhoades *et al* 2001, Högberg *et al* 2010, DeMarco *et al* 2011, Ruess *et al* 2013, Iwahana *et al* 2016). The net effect of these potential changes in nutrient supply and demand likely depends on local context, including soil organic matter stocks, permafrost stratigraphy, and hydrological conditions (Jorgenson and Osterkamp 2005, Loranty *et al* 2016, Sturm *et al* 2005, Tank *et al* 2020, Zolkos and Tank 2020, Abbott *et al* 2014). Given that initial and eventual effects of wildfire on lateral nutrient flux may be opposite (Fig. 1), we need observations of tundra ecosystem response across temporal and spatial scales (Parham *et al* 2013, Rodríguez-Cardona *et al* 2020, Ludwig *et al* 2018).

Quantifying nutrient dynamics at medium to large scales is challenging in any ecosystem (Bernhardt *et al* 2017, Pinay *et al* 2015), and particularly in permafrost regions where sites are remote and data are spatially and temporally sparse. This knowledge gap hinders process understanding of nutrient dynamics in complex permafrost landscapes (Lawrence *et al* 2011, Hurrell *et al* 2013, Kicklighter *et al* 2013), and consequently our ability to predict the permafrost climate feedback (McGuire *et al* 2018, Abbott *et al* 2016b, Chen *et al* 2018). One approach to quantify catchment-scale nutrient balance is to use streams as sensors of ecosystem processes (Brookshire *et al* 2009, Shogren *et al* 2019, Carey *et al* 2019, Zarnetske *et al* 2018). Stream nutrient concentrations and fluxes can indicate changes in terrestrial nutrient sources and sinks, providing a metric that integrates nutrient demand and uptake efficiency of terrestrial plants and microorganisms (Abbott *et al* 2018, Wymore *et al* 2019, Frei *et al* 2020). This approach has been widely used to assess terrestrial elemental balance in non-permafrost ecosystems, generating fundamental insights into ecosystem succession and other processes over time (Vitousek and

Reiners 1975, Fisher *et al* 1998, McClelland *et al* 2007, Lovett *et al* 2018). In high-latitude locations, this approach has been limited to a small number of watersheds (Temnerud and Bishop 2005, Metcalfe *et al* 2018, Kling *et al* 2000, Parham *et al* 2013, Malone *et al* 2018), largely due to logistical limitations (but see Shogren *et al* 2019).

In this context, we used an aerial sampling method to repeatedly measure stream chemistry in 42 tundra catchments in and around a large, 10-year-old burn scar on the North Slope of Alaska (Mack *et al* 2011, Jones *et al* 2009). We hypothesized that there would be lower nutrient concentrations and fluxes in burned compared to unburned watersheds because of the loss of soil organic matter (Jiang *et al* 2015a), rapid regrowth of vegetation (Bret-Harte *et al* 2013), and recovering active-layer thickness (Carey *et al* 2019). We tested these hypotheses in a multi-proxy framework (Abbott *et al* 2016a, Shogren *et al* 2019, Frei *et al* 2020), using individual physicochemical parameters and relationships among multiple parameters in stream water to infer the hydrology and biogeochemistry of the burned and unburned tundra watersheds.

Methods

The Anaktuvuk River fire

The study area is located on the North Slope of Alaska (Fig. 2), 150 km south of the Arctic Ocean and ~90 km northwest of the Toolik Field Station, associated with the Arctic Long-term Ecological Research (LTER) site. The area is underlain by continuous permafrost and has a mean annual air temperature of -10°C, with mean monthly temperature ranging from -15°C in January to 12°C in July. Mean annual precipitation is ~320 mm, with roughly a third falling as snow (Toolik Environmental Data Center Team 2019, King *et al* 2016).

The Anaktuvuk River fire was ignited by a lightning strike in mid-July of 2007 (Liu *et al* 2014). High air temperature, low precipitation, dry soils, and potentially site-specific characteristics allowed the fire to burn into early October (Liu *et al* 2014, Jones *et al* 2009). Eventually the fire burned 1,039 km^2 of Arctic tundra bounded by the Nanushuk and Anaktuvuk Rivers on the west, and the Itkillik River on the east (Fig. 2). The fire burned 80% of the area at moderate to extreme severities (Jones *et al* 2009). On average, the fire removed one third of the ~7,700 g C m^{-2} of organic matter and living biomass present before the burn (Mack *et al* 2011),

decreasing the organic-soil layer thickness from ~21 cm to ~15 cm (Mack *et al* 2011, Liu *et al* 2014, Rocha and Shaver 2011b).

In the first two years after the fire, numerous thermokarst features formed, and the land surface subsided by an additional 2 to 8 cm compared to adjacent, unburned areas due to active-layer thickening and thermokarst formation (Liu *et al* 2014). In the four years following the fire, burned areas had active-layer thickness that was 10 to 20 cm deeper than unburned areas (Rocha and Shaver 2011b), though differences in active-layer thickness between burned and unburned plots had decreased somewhat by our first sampling in 2017 (Carey *et al* 2019). After seven years (i.e. in 2014), thermokarst had affected 34% of the burn scar compared to only 1% of nearby unburned areas (Jones *et al* 2015).

There are very few measurements of surface water chemistry or lateral flux from this area. However, in 2011 (4 years after the burn), stream chemistry was measured in four reference and six burned watersheds within or near the Anaktuvuk River fire scar (Larouche *et al* 2015). The burned watersheds had higher dissolved organic carbon (DOC), ammonium (NH_4^+), phosphate (PO_4^{3-}), and total dissolved phosphorus and nitrogen than unburned watersheds, but lower nitrate (NO_3^-) (Larouche *et al* 2015).

The recovery of primary productivity occurred relatively quickly after the wildfire. Within four years, above-ground net primary productivity was equal in burned and unburned areas, though live biomass remained lower (Bret-Harte *et al* 2013). However, the recovered plant community in the burn scar differs from unburned areas, with more deep-rooted gramminoids, especially tussock-forming cotton grass (*E. vaginatum*) and sedges (e.g. *C. bigolowii),* an absence of lichens, and a shift in non-vascular species (Carey *et al* 2019, Bret-Harte *et al* 2013, Jandt *et al* 2012).

Experimental design and stream sampling methods

We implemented a repeated synoptic sampling design, collecting water samples from many streams at multiple points in time (McGuire *et al* 2014, Abbott *et al* 2018, Dupas *et al* 2019, Shogren *et al* 2019). Compared with more temporally intensive approaches that focus on a few locations, this spatially extensive design gave us more power to detect effects of the wildfire across different ecosystem gradients, though it reduced the breadth of parameters we could

measure (e.g. no water discharge or in situ sensor measurements). This approach has proven effective at quantifying medium- to large-scale ecosystem characteristics in remote locations, including the Arctic (Kling *et al* 2000, Crump *et al* 2012, Abbott *et al* 2015, Shogren *et al* 2019). To compensate for a lack of directly-measured covariates and ecosystem parameters for the sampling locations, we used a multi-proxy framework to constrain biogeochemical and hydrological processes based on water chemistry (Abbott *et al* 2016a, Pinay *et al* 2015, Kelleher *et al* 2019). For example, we inferred water flowpaths (depth of lateral flow relative to organic and mineral soil horizons) using ion concentrations and ratios (Keller *et al* 2010, Barker *et al* 2014), partitioning between evapotranspiration and lateral flow using stable isotopes in water (Berry *et al* 2018, Bush *et al* 2017), and sources of organic matter and nutrients (e.g. prefire soil versus postfire fixation) using optical properties of dissolved organic matter (DOM) and stable isotopes of carbon (C) and nitrogen (N) (Abbott *et al* 2016a, Malone *et al* 2018).

We sampled all major tributaries to the Anaktuvuk, Nanushuk, and Itkillik Rivers over a 110 km range (68.7° to 69.5° N) to control for variation in ecosystem characteristics, including elevation, latitude, topography, permafrost state, and watershed size (Fig. 2). Our sample sites included 42 accessible tributaries (21 burned and 21 unburned) in and around the burn scar, with watersheds ranging from 0.04 to 195 km^2 (mean and median areas of 34 and 21 km^2). These watersheds together drained 86% of the burn scar (Fig. 2). Burned and unburned watersheds tended to be smaller at the northern end of the sampling area because of the confluence of the Anaktuvuk and Nanushuk Rivers on the west side of the burn (Fig. 2).

The large geographic range of the sites and distance from the field station meant that landing the helicopter at each site was not possible because of fuel constraints. Consequently, we developed an aerial sampling method dubbed the Dübdeegan Dangle Maneuver (DDM), where we sampled the stream or river directly from the helicopter (Fig. S1). During the DDM, we press-fit a pre-washed, wide-mouth, 125 mL plastic bottle (HDPE) into a weighted cup at the end of a 4 m foldable aluminum sampling pole that we constructed from a broken camping table. As the pilot approached the site, we extended the pole and inserted the bottle under the water surface before the rotor wash from the helicopter disturbed the water surface to avoid stirring up sediment (Fig. S1 and linked video). After one or two seconds of filling, the bottle was retracted,

capped, and put into a cooler as the pilot navigated to the next site. This sampling method allowed us to fly the perimeter of the burn scar while collecting samples in two to four hours.

We collected samples in June, July, and August of 2017 and 2018, capturing three distinct periods in Arctic phenology (Shogren *et al* 2020). The June sampling occurred during the spring snowmelt period when river discharge was high, thaw depth was low, and primary productivity was very low. The July samples were collected during the peak growing season when discharge and thaw depth were moderate, and productivity was near its peak. The August sampling occurred after deciduous plant senescence when discharge was low, productivity was moderate, and thaw depth was greatest (Table 1; Fig. 3C). We collected samples from most of the sites for each sampling date, except for August of 2017, when a snowstorm and associated static discharge through the DDM pole to the helicopter airframe only allowed us to sample 19 of the sites (sample sizes reported in Table 1).

Water discharge and remotely sensed data

While no stream discharge stations exist within or near the burn scar, we measured continuous discharge in the Kuparuk River (68.636°, -149.39°) from mid-June to mid-September in 2017 and 2018. This location was 14 km from the nearest site and 118 km from the most distant site. At the Kuparuk location, we manually measured discharge periodically using the velocity-area method with a flow meter (SonTek Flow Tracker), and we measured water depth (stage) every 15 minutes with an autonomous pressure transducer (Onset HOBO, USA). We constructed a stage-discharge rating curve with these measurements, allowing estimation of continuous discharge across the flow season. To include the snowmelt period, when much of the annual discharge occurs, we completed the time series with data from the USGS Kuparuk River Station (15896000), approximately 100 km to the northeast of the burn scar. We calculated specific discharge (L m^{-2} day^{-1}) for each monitoring station and applied a linear conversion to the USGS data calculated during the period of overlap (i.e. mid-June to mid-September). While specific discharge could differ in and around the burn scar (King *et al* 2018, Lyon *et al* 2012), the relative magnitude of flow is likely similar, enabling calculation of flow-weighted means and estimates of lateral nutrient flux for the six samplings. We tested the assumption of similar specific discharge with water isotope measurements, which can indicate differences in evapotranspiration, storage, and runoff (Abbott *et al* 2016a).

To test our hypotheses about the relationship between catchment characteristics (e.g., size, burn severity, slope) and wildfire response, we delineated watersheds for each of the sampling locations using ArcGIS Pro (ESRI) with a 2-m resolution digital elevation model (DEM) (Porter *et al* 2018). We calculated elevation and slope directly from the DEM. We then intersected the watershed shapefiles with cloud-free Landsat and Sentinel images from before and after the burn to calculate several indices: the modified normalized difference water index (NDWI), normalized difference vegetation index (NDVI), and normalized burn ratio (dNBR) (Boelman *et al* 2011, Jones *et al* 2009, Kolden and Rogan 2013). We also calculated mean change in surface subsidence from 2006 to 2010 using published spatial data (Liu *et al* 2014).

Terrestrial plant and soil analyses

We quantified soil and plant C and N stocks in 2017 at an unburned, moderately burned, and severely burned site in or around the fire scar (Fig. 2). Burn severity was previously determined for these sites, based on dNBR (Rocha and Shaver 2011a). Following standard LTER protocols (Bret-Harte *et al* 2013), vegetation harvests were used to determine above and belowground biomass for each species. Samples were collected at the end of July, during the peak growing season. At each site, vegetation and soils were sampled randomly at 10-m intervals along two 100-m transects. Within a 10 × 40 cm quadrat, the entire vegetation and organic-soil layers (surface to mineral soil) was collected with a serrated bread knife and kept in plastic bags until processing. Upon arrival in the lab, quadrats were taken apart and plant material was sorted into aboveground leaf and woody biomass by species, and total belowground biomass. Leaf litter, coarse woody debris, and dead moss were also separated and measured. Samples were weighed after drying at 60 ^{o}C for 3 to 4 days. A subset of dried samples (~5 per plant species part or horizon and site) were finely ground and analyzed for C (%) and N (%) using an elemental analyzer (Costech, USA). We calculated site-level C and N content (g m^{-2}) using the area weighted values grouped by plant functional type: shrub, graminoid, lichen, and other (forbs, live moss, and unidentifiable).

To quantify soil C and N, we measured the depth of the peat and organic layer four times in each pit created by the biomass quadrat sampling. In half of the pits (i.e. 10), we extracted ~10 × 10 cm soil peat monoliths (i.e. “peat brownies”). Peat brownies were then wrapped in foil and transported to the lab, where they were dried and analyzed for C and N as previously described

for the aboveground biomass. For each brownie, we separated the peat and upper and lower organic soil based on color and texture. The bulk density estimates (g cm^{-3}) were multiplied by the in-field measurements of horizon thickness (cm) and soil C and N content (%) to determine soil stocks (g m^{-2}).

At three of the terrestrial sites, thaw depth was measured monthly from 2008 to 2019 as described in Rocha and Shaver (2011b). Briefly, a metal rod was used to make 40 measurements in a 100 × 40 m permanent grid at each site with an additional 36 measurements randomly taken along four 30-m transects. Thaw depth was noted from the top of the moss layer or soil if moss was not present. We interpreted the last thaw depth measurement from each year (last week of August or first week of September) as the active layer thickness (i.e. maximum annual thaw depth). Additionally, thaw depth was measured at 47 sites distributed within and near the burn scar in September of 2014 and 2019 (Fig. 2). At each of these survey sites, thaw depth was measured at 20 locations along a 20 m transect.

Aqueous analyses

Upon returning to the lab, unfiltered water samples were immediately analyzed with a spectrophotometer (s::can, Austria) for UV-Vis absorbance (190-750 nm) and turbidity. We then filter-sterilized 60 mL of each sample with a pre-rinsed cellulose acetate membrane filter (0.2 µm-pore size). Samples were refrigerated until analysis within one month. Filter-sterilized samples were analyzed for anions, cations, dissolved elements, water isotopes, C, and total dissolved N (TDN). We used ion chromatography (ThermoFisher Dionex, USA) to quantify anions and cations, including fluoride (F^-), acetate ($C_2H_3O_2^-$), formate ($CH_2O_2^-$), chloride (Cl^-), nitrite (NO_2^-), bromide (Br^-), sulfate (SO_4^{2-}), PO_4^{3-}, lithium (Li^+), sodium (Na^+), potassium (K^+), magnesium (Mg^{2+}), and calcium (Ca^{2+}). NH_4^+, and NO_3^- were determined colorimetrically using an autoanalyzer (LACHAT, USA). We summed NO_3^-, NO_2^-, and NH_4^+ to calculate dissolved inorganic N (DIN). We used an inductively coupled plasma optical emissions spectrometer (Thermo Scientific 7400 series, USA) to quantify concentrations of dissolved elements (Al, As, B, Ba, Ca, Cd, Co, Cr, Cu, Fe, K, Mg, Mn, Mo, Na, Ni, P, Pb, S, Se, Si, Sr, Ti, V, and Zn). We replaced values that fell below the limit of detection (LOD) with the LOD/2. We measured DOC, dissolved inorganic C (DIC), and TDN on an elemental analyzer (Elementar, Germany) after evolution to CO_2 or NO. We used cavity ringdown spectroscopy (Los Gatos Research, USA) to

quantify stable isotope ratios of hydrogen (δD) and oxygen ($\delta^{18}O$) in water relative to Vienna Standard Mean Ocean Water (VSMOW). The analyzer had a precision of ±1 for δD and ±0.4 for $\delta^{18}O$. We calculated the local meteoric water line from published measurements of precipitation in the nearby Kuparuk River watershed (Harms and Godsey 2017).

In 2018, we additionally froze a 30-mL subsample of 0.2-µm filtered water for stable isotope analysis of DOC and NO_3^- at the UC Davis Stable Isotope Facility. The $\delta^{13}C$ of DOC was quantified after digestion to CO_2 with an isotope ratio mass spectrometer (Sercon Ltd., UK). The $\delta^{15}N$ and $\delta^{18}O$ of NO_3^- were quantified via bacterial denitrification (Sigman *et al* 2001), with the evolved N_2O measured on a mass spectrometer (Bremen, Germany).

We calculated dissolved organic N, phosphorus, and sulfur by difference between the total elemental amount and the inorganic solute (i.e. DON = TDN – DIN, DOP = P – PO_4^{3-}, and DOS = S – SO_4^{2-}). In addition to the individual solute concentrations, we calculated ratios of several geogenic solutes (Ca^{2+}, Mg^{2+}, Sr^{2+}, Na^+, SO_4^{2-}, and Ba^{2+}) that have been found in some regions to indicate depth of hydrological flow associated with seasonal and interannual changes in permafrost (Table S1; Keller *et al* 2010, Lehn *et al* 2017, Barker *et al* 2014).

To calculate optical metrics of DOM composition (Table S1), we measured excitation emission matrices (EEMs) with a scanning fluorometer (Horiba, Japan). Scans were performed using a 150-watt Xenon lamp with varying integration times between 0.5–5 minutes depending on absorbance. Following standard methods (Cory *et al* 2010), all samples were corrected for inner filter effects, Rayleigh scatter, and blank subtraction in MATLAB™ (version 6.9; MathWorks, USA). We analyzed the EEMs to calculate several common indices of DOM composition, including biological index (BIX), humification index (HIX), fluorescence index (FI), E2/E3 index, and specific UV absorbance at 254 nm ($SUVA_{254}$) (McKnight *et al* 2001, Weishaar *et al* 2003, Fellman *et al* 2010, Kellerman *et al* 2018, Gabor *et al* 2014, 2015). The calculations and interpretations of these metrics are detailed in Table S1.

Statistical analyses and calculations

We tested for relationships between water chemistry and catchment characteristics (including burn extent and severity) with Pearson correlation coefficients (r). Because the dataset included multiple measurements from the same sites, we calculated the site mean (flow-weighted

and unweighted) for each parameter prior to calculating r. The flow-weighted values are more relevant to questions of mass balance (e.g. nutrient flux) because they most represent the high-flow sampling during snowmelt in June, while the unweighted values are more sensitive to changes throughout the year, including when flow was lower in July and August (Table 1). We calculated r for organic and inorganic nutrients, optical properties, stable isotopes, and geochemical ratios, using a decision criterion of $\alpha = 0.05$. Based on the high level of co-linearity observed among ions (see next paragraph), we calculated r for 6 representative solutes (Cl^-, Br^-, F^-, K^+, Mg^{2+}, Sr^{2+}) and the sum of anions and cations.

Because water chemistry parameters were often related in nonlinear ways, we calculated Spearman rank correlations (ρ) to quantify relationships among parameters (optical, chemical, and isotopic). Before calculating ρ, we scaled the data within sampling date (subtracting the mean and dividing by the standard deviation) to allow comparison of spatial differences among sites rather than temporal differences due to seasonality and discharge across the two years. Because of the larger number of comparisons, we used a decision criterion of $\alpha = 0.01$ when assessing statistical significance.

For each year (i.e. 2017 and 2018), we estimated annual organic nutrient flux from the unburned and burned area on an areal basis (mg m^{-2} $year^{-1}$). To do this, we first calculated the flow- and area-weighted mean concentrations for the entire burned and unburned watershed areas for each year. We then multiplied these concentrations by the cumulative specific discharge for that year (L m^{-2} $year^{-1}$). We recognize that these inferred discharge data are unlikely to provide high-precision estimates of flux (Shogren *et al* 2020, Minaudo *et al* 2017, Lyon *et al* 2012). However, recent observations of the temporal persistence of spatial patterns in stream networks (Shogren *et al* 2019, Abbott *et al* 2018) and especially the high level of spatial replication in this study (Fig. 2) suggest that relative comparisons among burned and unburned watersheds are robust.

We used analysis of variance (ANOVA) to test for differences in terrestrial stocks of C and N among the unburned, moderately burned, and severely burned sites. We considered the 20 sampling locations (10 for peat and SOM) from each site as the experimental unit. For post hoc comparisons, we applied a Bonferroni correction for a familywise α of 0.05. For the ANOVA

and Pearson analyses, we visually inspected residual plots for deviations from normality, linearity, and homoscedasticity.

Statistical analyses and visualizations were performed in R (R Core Team 2018, Wickham *et al* 2020). The meteorological data are available from the Toolik Environmental Data Center (Toolik Environmental Data Center Team 2019), and all chemistry and discharge data are attached.

Results

Interannual variation and differences among catchments

The two years of the sampling were very distinct hydrologically and climatically (Fig. 2; Table 1). Total specific discharge was 319 L m^{-2} $year^{-1}$ in 2017 and 702 L m^{-2} $year^{-1}$ in 2018. Specific discharge was higher in 2018 because of a larger snowmelt peak, large rain events in September, and more precipitation overall (236 mm in 2017 versus 405 mm in 2018, June-September). The sampling dates captured most of this interannual and seasonal variability of flow, spanning 76% of the observed variation in river discharge across the sampling years (Fig. 2B and Table 1). The flow season of 2017 was warmer than 2018, with a May-September mean air temperature of 5.3°C in 2017 and 4.0°C in 2018. At the unburned and severely burned terrestrial sites, active layer thickness was shallower in 2018 than in 2017, though it was similar across years at the moderately burned site (Fig. 3A).

The spatial analysis of watershed characteristics showed that burned and unburned watersheds were comparable for most topographic and surficial parameters (e.g. size, surface wetness, water coverage, location), though the slope and elevation happened to be slightly lower in burned watersheds, attributable to the geometry of the fire scar (Figs. S2 and 2). Greenness (NDVI) based on satellite imagery from 2017 was similar for burned and unburned watersheds, indicating recovery of the aboveground plant community. As expected, burn severity (dNBR) based on satellite imagery from 2006 and 2008 was much higher in the burned watersheds, with a mean near 400 (severe burn) compared to 0 (no burn) for the unburned watersheds (Fig. S2). The burned watersheds also showed substantial subsidence (mean of 3.9 cm in burned versus 0 cm in unburned watersheds) based on data from 2010 (Liu *et al* 2014). The burn parameters (i.e. burn extent, severity, and subsidence) were strongly correlated with each other ($r > 0.8$, $p <$

0.001; Table S2). Several of the watershed characteristics showed latitudinal gradients, with elevation, slope, and NDVI decreasing to the north, and the burn parameters and surface water increasing to the north, partially attributable to the latitudinal distribution of burned and unburned watersheds (Table S2).

Active layer thickness at the three terrestrial sites was greater at the burned locations across the 12 years of monitoring, with 2008–2019 means of 52.8 cm (±8.7; SD), 61.2 cm (±10.8), and 64.4 cm (±11.7) for the unburned, moderately burned, and severely burned sites, respectively (Fig. 3A). Active layer thickness at the severely burned sites showed some signs of recovery, with depths converging toward the moderately burned values in 2016–2019 (Fig. 3A). Conversely, there was greater active layer thickness and difference between burned and unburned locations in 2019 versus 2014, based on the thaw depth survey of 47 sites (Fig. 3B).

Terrestrial carbon and nitrogen stocks

Total ecosystem C and N to the mineral soil averaged 9,800 g C m^{-2} (±910; SE) and 310 g N m^{-2} (±20) at the unburned site, 9,300 g C m^{-2} (±910) and 200 g N m^{-2} (±22) at the moderately burned site, and 6,800 g C m^{-2} (±950) and 250 g N m^{-2} (±24) at the severely burned site. Assuming similar pre-burn C and N, this represented mean C decreases of 5.7 and 31% for the moderately and severely burned sites, respectively, and mean N decreases of 34 and 18% relative to the unburned site (Fig. 4A and 4B). Across all sites, belowground stocks (primarily peat and organic soil) accounted for an order of magnitude more C and N than aboveground stocks (Fig. 4A and 4B). Aboveground biomass was similar across burn severities, indicating recovery of aboveground plant C and N, though the moderately burned site had less biomass (Fig. 4A). Belowground biomass and soil C and N were generally lower at the burned sites, with 22 to 85% less C and N than the unburned sites (Fig. 4A and 4B). The overall C and N percent was not significantly different across classes (Fig. 4C). Graminoids made up a proportionally larger fraction of ecosystem C and N in both the moderately and severely burned sites (Fig. 4A).

Relationships between watershed characteristics and water chemistry

The unweighted and flow-weighted Pearson correlations among water chemistry and watershed characteristics were highly consistent for most parameters (Tables S3 and S4). Likewise, the Spearman correlations among parameters were highly consistent across burned and

unburned watersheds (Figs. S3 and S4). For simplicity, we hereafter refer to the unweighted means of the entire sample, except where specified otherwise.

The site means of all dissolved organic nutrients were positively correlated with burn severity (Fig. 5A). Organic nutrients were also positively correlated with burn extent and subsidence, though not as strongly as with severity (Fig. 6). There were several other correlations between specific organic nutrients and non-fire watershed characteristics (e.g. DOC with NDWI), but these relationships were weaker and largely attributable to the distribution of the fire scar across different landscape types. In contrast, none of the inorganic nutrients or isotopic parameters (i.e. isotopes of NO_3^-, DOC, and water) were correlated with the burn parameters, except dissolved silica (negatively correlated with extent and severity) and water isotopes (positively correlated with subsidence; Figs. 5B and 6). Two of the six optical properties of DOM—$SUVA_{254}$ and FI—were correlated with the burn parameters, indicating a higher proportion of aromatic DOM and more plant versus microbial DOM sources in burned watersheds, respectively (Fig. 5B). Optical properties were more correlated with nonburn parameters, particularly NDWI (Fig. 6).

The sums of anions and cations were not correlated with burn extent or severity, but all ions were positively correlated with subsidence (Fig. 6). Br^-, F^-, and K^+ were also positively correlated with burn extent and severity, though less than with subsidence. None of the geochemical ratios (e.g. Ca^{2+}:Sr^{2+}; Table S1) were correlated with the burn parameters (Fig. 6). Most of the solutes and geochemical ratios showed significant negative correlations with elevation and slope, and consequently positive correlations with latitude (Fig. 6; Table S2).

Seasonal differences in water chemistry

For both burned and unburned watersheds, organic nutrient concentrations increased seasonally, with the largest increases between June and July, indicating a negative concentration-discharge relationship (Fig. 7A). Inorganic nutrients did not show consistent seasonal patterns (Fig. 7B). DIN and PO_4^{3-} concentrations were much lower than their organic counterparts (i.e. DON and DOP), and DIC was somewhat lower than DOC (Fig. 7B). However, SO_4^{2-} was much higher than DOS (Fig. 7B). Inorganic nutrients were strongly left skewed (occasional extreme values), particularly PO_4^{3-} and SO_4^{2-} (Fig. 7B).

444 The optical metrics of DOM properties showed various seasonal patterns (Fig. 7C). The
445 patterns were generally clearer in 2018, the wetter and cooler year (Table 1). $SUVA_{254}$ and FI,
446 the two optical properties that varied with burn extent and severity (Figs. 5 and 6), both showed
447 seasonal increases, indicating a shift towards more aromatic and microbially modified DOM
448 (Table S1). HIX also increased consistently in both years, indicating more degraded DOM with
449 lower H:C ratios. The other parameters showed different patterns across years (E_2/E_3, BIX) or no
450 change (S_R; Fig. 7C).

451 Stable isotopes of DOC and NO_3^- did not show consistent trends through the season,
452 except for $\delta^{18}O\text{-}NO_3^-$, which was substantially lower for both burned and unburned watersheds
453 in the August sampling (Fig. 8A). $\delta^{13}C$-DOC was not correlated with DOC concentration for
454 burned or unburned watersheds ($\rho = -0.16$, $p = 0.3$; Figs. 8B and S3). The relationship between
455 $\delta^{18}O$ and $\delta^{15}N$ of NO_3^- was consistent across burn status ($\rho = 0.71$, $p < 0.01$), suggesting similar
456 sources and removal pathways of N (Fig. 8B).

457 Water isotopes were strongly depleted ($\delta^{18}O < -15$ ‰, $\delta D < -120$ ‰), consistent with the
458 high latitude (Fig. 9). Isotopic values showed strong seasonal increases, indicating a shift from
459 snow- to rain-dominated runoff (Fig. 9A). The seasonal increase was initially more rapid in the
460 warmer, dryer year of 2017. However, the snow event on the week of the sampling in August
461 resulted in substantially lower isotopic values, demonstrating the low storage and short
462 hydrological residence times of these watersheds (Fig. 9A). The local evaporation lines
463 (relationship between $\delta^{18}O$ and δD in stream water) were consistent for unburned and burned
464 watersheds (Fig. 9B). Both lines plotted just below the local meteoric water line, suggesting
465 limited evapotranspiration compared to runoff, supporting the assumption of similar specific
466 discharge across burned and unburned watersheds.

467 Most of the ions showed increases through the season, except for K+, which showed a
468 large pulse during snowmelt (June), and Cl^-, which was higher in the peak growing season (July)
469 both years (Fig. S5). As expected, the Ca^{2+}:Sr^{2+} ratio decreased systematically over the flow
470 season, indicating deeper flow of water through the soil profile (Fig. S5). However, the other
471 ionic ratios potentially associated with thaw depth did not show consistent seasonal patterns (Fig.
472 S5).

473 *Lateral flux of organic nutrients*

All organic nutrients showed substantially higher lateral flux in burned watersheds (Table 2). This was attributable to the significant correlations of organic nutrient concentrations with burn extent, severity, and subsidence (Figs. 4 and 5; Tables S3 and S4). The interannual mean flux of DOC, DON, DOP, and DOS was 25 to 65% higher in burned watersheds compared to unburned watersheds (Table 2). For unburned and burned watersheds, organic nutrient fluxes were approximately twice as high in 2018 than 2017, due to greater runoff. Also, relative differences in organic nutrient flux between burn and unburned watersheds were greater for all nutrients except DOC in 2018 (Table 2).

Discussion

To investigate how tundra wildfire can affect lateral nutrient export, we quantified nutrient concentrations and a broad suite of water chemistry parameters from 42 watersheds in and around the >1,000 km^2 Anaktuvuk River fire in northern Alaska. Contrary to our hypothesis that high terrestrial nutrient demand and lower C and N stocks would decrease lateral nutrient export, burned watersheds had substantially higher lateral flux of organic nutrients. Below, we discuss what could be causing these differences in lateral nutrient flux and what this nutrient loss might mean for tundra ecosystems recovering from wildfire.

Evidence of persistent, plant-mediated export of permafrost nutrients

The observed lateral release of nutrients was unexpected on two accounts. First, this ecosystem is still recovering from a major disturbance that substantially decreased soil and biomass nutrient stocks (Mack *et al* 2011, Jiang *et al* 2015a, Bret-Harte *et al* 2013). General theory and studies from this region predict strong net nutrient retention during this period of ecosystem recovery (Malone *et al* 2018, Lovett *et al* 2018, Pearce *et al* 2014, Rastetter *et al* 2020). Second, when lateral nutrient loss does occur in nutrient-limited permafrost ecosystems, it is usually due to temporal and spatial mismatches in supply and demand. For example, water flow below the rooting zone or outside of the growing season (i.e. shoulder seasons) can result in substantial nutrient loss from nutrient-limited permafrost regions (Jones *et al* 2005, Treat *et al* 2016, Harms and Jones 2012, Shogren *et al* 2020, Blume-Werry *et al* 2016, p). However, these scenarios of deeper and longer flow predict lower organic to inorganic nutrient ratios, more processed DOM, higher solutes, and enriched stable isotope values for DOC and NO_3^- (MacLean *et al* 1999, Harms and Jones 2012, Malone *et al* 2018, Lehn *et al* 2017, Keller *et al* 2010, Mu *et*

504 *al* 2017, Toohey *et al* 2016, Frey and McClelland 2009, Treat *et al* 2016, Shogren *et al* 2020,
505 Wologo *et al* 2020).

506 In every case, the patterns predicted by the deep flowpath and shoulder season hypotheses of
507 nutrient flux were the opposite of what we observed. For example, the optical proxies and DOC
508 isotopes suggested that the DOM and constituent organic nutrients are derived from postfire
509 plant material in burned watersheds rather than directly from deeper organic matter activated by
510 the wildfire (Figs. 1 and 10). Likewise, the consistent differences in organic nutrient
511 concentrations before, during, and after peak growing season, despite distinct soil nutrient
512 dynamics (Buckeridge *et al* 2013, Melle *et al* 2015, McLaren *et al* 2017, Darrouzet-Nardi *et al*
513 2019), suggest that short-term terrestrial demand is not directly regulating lateral nutrient flux
514 (Fig. 7). Additionally, the isotopes of NO_3^- indicate that lateral N flux is not being driven by
515 postfire N fixation (Malone *et al* 2018). Finally, similar inorganic nutrient concentrations and the
516 higher organic to inorganic nutrient ratios in burned watersheds suggests nutrient sourcing from
517 organic horizons rather than mineral horizons. Regarding interpretation of nutrient patterns in
518 streams, we point out that inorganic nutrient release from terrestrial environments could be
519 obscured by uptake and mineralization in the aquatic environment, which is highly nutrient
520 limited (Rodríguez-Cardona *et al* 2020, Kendrick *et al* 2018, Kling *et al* 2000), whereas organic
521 nutrients move more conservatively through small Arctic watersheds such as these (Shogren *et al*
522 2019, Abbott *et al* 2016a).

523 We hypothesize that the elevated organic nutrient flux from areas affected by the wildfire is
524 caused by cumulative plant and mycorrhizal uptake of nutrients released from thawed permafrost
525 (Fig. 1). Rather than directly leaching nutrients from the thaw front, as predicted by the deep and
526 shoulder season hypotheses, this plant-mediated hypothesis explains the sustained nutrient loss
527 despite ecosystem succession, recovering active layer thickness, and intense terrestrial nutrient
528 demand (Bret-Harte *et al* 2013, Jiang *et al* 2015a, Carey *et al* 2019). Despite the loss of
529 approximately four centuries worth of nutrients during the wildfire (Mack *et al* 2011, Bret-Harte
530 *et al* 2013), over the first decade of postfire recovery, plants could have accessed nutrients
531 released by thermokarst formation (i.e. subsidence; Liu *et al* 2014, Jones *et al* 2015) and
532 increased active layer thickness (Carey *et al* 2019, Rocha and Shaver 2011b). The stronger and
533 more consistent correlations between organic nutrients and burn severity versus subsidence (Fig.

6) suggest that active layer thickening is more influential than thermokarst formation, though both processes are likely at play. Tundra plants—especially the deep-rooted graminoids more dominant in the burn scar (Fig. 5)—readily take up nutrients released at the thaw front (Hewitt *et al* 2015, Salmon *et al* 2018, Keuper *et al* 2017, Carey *et al* 2019). For example, detailed characterization of the plant community four years postfire showed lower C:N ratios in regrowth followed by greater allocation to belowground biomass (Bret-Harte *et al* 2013). While we do not have detailed surface water data, measurements from the same time period suggest that enhanced lateral nutrient flux was already occurring four years postfire (Larouche *et al* 2015). While the overall stocks of C and N are still lower in the burned watersheds (Fig. 4), new growth from plants accessing thaw-front nutrients could be producing fresh organic matter that is more easily solubilized and leached, such as litter and fine roots (Zarnetske *et al* 2018, Wickland *et al* 2007, Neilson *et al* 2018, Wickland *et al* 2018, O'Donnell *et al* 2013, 2016a). Additionally, root exudates in the burned watersheds could be enhancing mineralization and potentially dissolution of peat and organic soil (Keuper *et al* 2020), further fueling lateral loss of organic nutrients.

If this phenomenon of plant-mediated nutrient flux is widespread, it would explain the widely observed long-term increase in both DOM and solutes from most permafrost catchments where data are available (Frey and McClelland 2009, Mann *et al* 2016, Tank *et al* 2016, Wauthy *et al* 2018, Toohey *et al* 2016, Drake *et al* 2018, Holmes *et al* 2012, Frey *et al* 2007, Kendrick *et al* 2018). The simultaneous increase in both DOM and solutes is contrary to the active layer thickening hypothesis, which predicts decreased DOM with permafrost degradation due to longer residence times and enhanced mineralization and sorption of DOM in mineral soil layers (Striegl *et al* 2005, Kicklighter *et al* 2013, Laudon *et al* 2013, Mu *et al* 2017, MacLean *et al* 1999). Thermokarst formation, which delivers both DOM and solutes to river networks, has been proposed as one explanation to this paradox (Abbott *et al* 2015, Bowden *et al* 2012, Coch *et al* 2019), but recent observations show that only some thermokarst features increase DOM delivery, likely based on local periglacial history and vertical distribution of organic matter (Zolkos and Tank 2020, Tank *et al* 2020). Additionally, most of the DOM in Arctic and Boreal surface waters is relatively modern (e.g. fixed within the last century), while thermokarst DOM is largely pre-modern (Wild *et al* 2019, Mollenhauer *et al* 2019, Ewing *et al* 2015, Burd *et al* 2018, Gaglioti *et al* 2014, Raymond *et al* 2007, Wang *et al* 2018), further suggesting that recent plant growth is fueling increases in DOM flux from the permafrost region.

In addition to thermokarst formation, plant-mediated nutrient flux is a complementary hypothesis explaining the simultaneous increase in lateral DOM and solute flux. Areas undergoing active layer deepening could be losing solutes via deeper flow and thermokarst, while plant growth and regrowth fuel increasing lateral DOM flux. Solute and nutrient increases have primarily been attributed to deepening of the seasonally-thawed active layer (Kawahigashi *et al* 2006, Harms and Jones 2012, Walvoord and Kurylyk 2016), which allows water to move deeper in the soil profile where it interacts with solute-rich permafrost (Petrone *et al* 2006, Reyes and Lougheed 2015, O'Donnell *et al* 2016b). The results from our study, however, suggest that surface subsidence is driving solute flux, while plant regrowth and nutrient mobilization from areas of deeper active layer are regulating organic nutrient flux. While these results are limited to a single region, they demonstrate the interactions between gradual and abrupt thaw, highlighting the need to simulate these processes together (Turetsky *et al* 2020, Abbott *et al* 2015).

Implications of lateral nutrient loss for local ecosystems and global climate feedbacks

Our results reinforce evidence that permafrost degradation and wildfire can trigger substantial nutrient loss from ecosystems that are already nutrient-limited (Mack *et al* 2008, Betts and Jones 2009, Pearce *et al* 2014, Abbott *et al* 2015). Although we do not have complete budgets for most of the nutrients in this study, lateral N loss from burned watersheds is 2- to 10-fold higher than estimates of N fixation and atmospheric deposition for this region (Weiss *et al* 2005, Jiang *et al* 2017, Mack *et al* 2011). In combination with vertical N losses that we did not quantify (e.g. denitrification and volatilization; Voigt *et al* 2020, Malone *et al* 2018, Abbott and Jones 2015), our observations suggest that wildfire triggers a long-term and substantial nutrient deficit. This sustained loss could have contrasting consequences at global, regional, and local scales.

Starting at the global scale, predicting the permafrost C feedback to the Earth's climate depends on accurate estimates of greenhouse gas release and uptake in permafrost ecosystems (Schuur *et al* 2015). Most Earth system models project substantial accumulation of C in living biomass and soil organic matter in the permafrost zone, sometimes sufficient to offset all greenhouse gas release from permafrost (i.e. a net stabilizing feedback from the permafrost zone; McGuire *et al* 2018). However, most of these models are not fully coupled with nutrient cycles, and they often predict strong CO_2-fertilization effects and rapid ecosystem transitions (e.g.

595 tundra to taiga), despite a lack of observations of these dynamics in current or past permafrost
596 ecosystems (Abbott *et al* 2016b, Oberbauer *et al* 1986, Wieder *et al* 2015, 2019, Fisher *et al*
597 2019). If increased wildfire in Arctic tundra consistently increases lateral nutrient loss, the
598 capacity of permafrost ecosystems to offset greenhouse gas release could be substantially
599 diminished. Conversely, lower nutrient availability following wildfire could decrease N_2O
600 production, reducing this non-carbon greenhouse gas (Voigt *et al* 2020).

601 At the regional scale, sustained lateral flux of nutrients following wildfire could alter
602 recipient ecosystems in aquatic, estuarine, and marine environments. The C balance and food
603 webs of these ecosystems are highly sensitive to C, N, phosphorus, sulfur, and silica (McClelland
604 *et al* 2012, Carey *et al* 2019, Slavik *et al* 2004, Kendrick *et al* 2018, Vancoppenolle *et al* 2013,
605 Arrigo *et al* 2012), all of which were strongly affected by the wildfire in our study. The addition
606 of bioavailable C and nutrients could affect C balance and light dynamics, potentially increasing
607 or decreasing greenhouse gas release depending on interactions among organic matter
608 production, breakdown, and environmental conditions (Wologo *et al* 2020). Depending on the
609 future extent of wildfire in areas of the tundra biome where it has previously been rare (Abbott *et*
610 *al* 2016b, Rocha *et al* 2012, Jones *et al* 2013), plant-mediated nutrient loss could alter regional
611 nutrient budgets, influencing C balance and habitat in donor and recipient ecosystems.

612 At the local scale, long-term nutrient deficits could slow encroachment of shrubs and forest
613 into the tundra biome. Because the tundra-taiga transition is defined by nutrient status more than
614 temperature, mechanisms that reduce nutrient availability effectively increase the resilience of
615 tundra ecosystems to climate change (Bret-Harte *et al* 2013, Wein and Bliss 1973, Zimov *et al*
616 2009). While tundra wildfire can trigger ecosystem transitions in areas that are warmer and more
617 nutrient rich (Jandt *et al* 2012, Landhausser and Wein 1993), our study suggests that cold and
618 nutrient-poor tundra areas may be resilient to forest encroachment and shrub expansion (Myers-
619 Smith *et al* 2011, Frost *et al* 2013, Zamin and Grogan 2012, Wein and Bliss 1973), at least on
620 decadal timescales. Postfire nutrient loss could be an important resilience mechanism—a way of
621 shedding excess nutrients as permafrost degrades—similar to how conifer forests shunt nutrients
622 during wildfire (Tierney *et al* 2019). Alternatively or additionally, nutrient loss could convey
623 adaptive advantages to the graminoids responsible for it, in this case primarily *E. vaginatum*
624 (Bret-Harte *et al* 2013, Mack *et al* 2011, Wein and Bliss 1973). *E. vaginatum* is already known

to be an ecosystem engineer, lowering the temperature of underlying soil and permafrost by several degrees (Shur and Jorgenson 2007, Loranty *et al* 2018). If *E. vaginatum* is facilitating nutrient loss from burned tundra, it could be maintaining the oligotrophic nutrient conditions where it dominates tundra plant communities via nutrient shunting.

On a related topic, we emphasize that understanding the local to global impacts of permafrost wildfire on C dynamics requires better integration of hydrological processes into C and nutrient cycles (Zarnetske *et al* 2018, Lawrence *et al* 2015, Douglas *et al* 2020, Neumann *et al* 2019, Jorgenson *et al* 2013). River runoff varied by more than a factor of two between the two years of our study, with the amount and type of lateral nutrient loss following suit (Table 2). This demonstrates how constraining the amount, timing, and flowpath of water through these ecosystems is crucial to determining local nutrient balance and ultimately, the global permafrost climate feedback (Laudon *et al* 2013, Vonk *et al* 2015, Tank *et al* 2020).

Wildfire effects on lateral flux depend on initial stocks and successional dynamics

While there are few studies of lateral nutrient flux following tundra wildfire, the available observations from other regions provide crucial context for our results (Larouche *et al* 2015, Parham *et al* 2013, Rodríguez-Cardona *et al* 2020, Ludwig *et al* 2018). Studies of Siberian tundra and taiga wildfires have found a more expected pattern of a pulse of inorganic nutrients, followed by the gradual recovery of organic nutrient concentrations over several decades (Rodríguez-Cardona *et al* 2020, Parham *et al* 2013). This aligns with terrestrial observations of relatively larger decreases in organic matter stocks in these areas (Ludwig *et al* 2018) compared to what we observed on the North Slope. We suggest that this difference could be due to greater active layer thickness and lower initial C and nutrient stocks in ecosystems with much more frequent wildfires (Kirdyanov *et al* 2020). The North Slope of Alaska has a very thin active layer and extremely infrequent wildfires, like much of the continuous permafrost zone (Rocha *et al* 2012, Jones *et al* 2013). These conditions could lead to greater postfire nutrient sources and enhanced importance of surface vegetation in driving lateral fluxes because the permafrost table largely constrains flow to the rooting zone (Parham *et al* 2013, Neilson *et al* 2018).

The importance of local ecological conditions in regulating the response to wildfire is further apparent in the geochemical data from our study. For example, only one of the several geochemical ratios that have been used as tracers of thaw depth in areas not far from the

Anaktuvuk River fire (Keller *et al* 2010, Lehn *et al* 2017, Barker *et al* 2014) showed the expected seasonal patterns (i.e. Ca^{2+}:Sr^{2+}; Fig. 11C). This should not be surprising given the heterogeneity of periglacial history and near-surface geology of the permafrost zone (Tank *et al* 2020, Abbott *et al* 2014, Larouche *et al* 2015, Strauss *et al* 2017). Considering this diversity of ecological context is crucial to accurate scaling and identification of robust trends. While it may still be premature, the superposition of global-scale soil and vegetation profiles with projected fire frequency (Olefeldt *et al* 2016, Hugelius 2012, Kolden and Rogan 2013), could allow empirical and potentially mechanistic modeling of the effects of wildfire on lateral nutrient flux. In any case, considering differences in organic matter stocks, vegetation types, surficial geology, hydrology, and active layer thickness is crucial to projecting the response of C and nutrient dynamics to tundra wildfire across the permafrost zone.

Acknowledgements

This work was supported by the National Science Foundation award numbers 1916565, 1916567, 1916576, 1906381, DEB 1026843, and DEB 1556772. We thank the Toolik Field Station for world-class logistical support and the Toolik GIS Office for initial watershed delineation and analysis. We thank Natasha Griffith, Salvatore Curasi, Meghan Christie, Ian Klupar, Cameron MacKenzie, and Heidi Golden for dedicated and cheerful field and lab assistance. Rachel Buck and Andrew Luymes carried out the nutrient and ICP analyses in the BYU Environmental Analytical Laboratory. Kevin Rey performed the measurements of water isotopes at the BYU Geochemistry Lab. We thank Bianca Rodríguez-Cardona for input on an early version of the manuscript.

References

Abbott B W, Baranov V, Mendoza-Lera C, Nikolakopoulou M, Harjung A, Kolbe T, Balasubramanian M N, Vaessen T N, Ciocca F, Campeau A, Wallin M B, Romeijn P, Antonelli M, Gonçalves J, Datry T, Laverman A M, de Dreuzy J-R, Hannah D M, Krause S, Oldham C and Pinay G 2016a Using multi-tracer inference to move beyond single-catchment ecohydrology *Earth-Science Reviews* **160** 19–42

Abbott B W, Gruau G, Zarnetske J P, Moatar F, Barbe L, Thomas Z, Fovet O, Kolbe T, Gu S, Pierson-Wickmann A-C, Davy P and Pinay G 2018 Unexpected spatial stability of water chemistry in headwater stream networks *Ecol Lett* **21** 296–308

685 Abbott B W and Jones J B 2015 Permafrost collapse alters soil carbon stocks, respiration, CH4, and N2O
686 in upland tundra *Glob Change Biol* **21** 4570–87

687 Abbott B W, Jones J B, Godsey S E, Larouche J R and Bowden W B 2015 Patterns and persistence of
688 hydrologic carbon and nutrient export from collapsing upland permafrost *Biogeosciences* **12**
689 3725–40

690 Abbott B W, Jones J B, Schuur E A G, III F S C, Bowden W B, Bret-Harte M S, Epstein H E, Flannigan M D,
691 Harms T K, Hollingsworth T N, Mack M C, McGuire A D, Natali S M, Rocha A V, Tank S E, Turetsky
692 M R, Vonk J E, Wickland K P, Aiken G R, Alexander H D, Amon R M W, Benscoter B W, Bergeron
693 Y, Bishop K, Blarquez O, Bond-Lamberty B, Breen A L, Buffam I, Cai Y, Carcaillet C, Carey S K,
694 Chen J M, Chen H Y H, Christensen T R, Cooper L W, Cornelissen J H C, Groot W J de, DeLuca T H,
695 Dorrepaal E, Fetcher N, Finlay J C, Forbes B C, French N H F, Gauthier S, Girardin M P, Goetz S J,
696 Goldammer J G, Gough L, Grogan P, Guo L, Higuera P E, Hinzman L, Hu F S, Hugelius G, Jafarov E
697 E, Jandt R, Johnstone J F, Karlsson J, Kasischke E S, Kattner G, Kelly R, Keuper F, Kling G W,
698 Kortelainen P, Kouki J, Kuhry P, Laudon H, Laurion I, Macdonald R W, Mann P J, Martikainen P J,
699 McClelland J W, Molau U, Oberbauer S F, Olefeldt D, Paré D, Parisien M-A, Payette S, Peng C,
700 Pokrovsky O S, Rastetter E B, Raymond P A, Raynolds M K, Rein G, Reynolds J F, Robard M,
701 Rogers B M, Schädel C, Schaefer K, Schmidt I K, Shvidenko A, Sky J, Spencer R G M, Starr G,
702 Striegl R G, Teisserenc R, Tranvik L J, Virtanen T, et al 2016b Biomass offsets little or none of
703 permafrost carbon release from soils, streams, and wildfire: an expert assessment *Environ. Res.*
704 *Lett.* **11** 034014

705 Abbott B W, Larouche J R, Jones J B, Bowden W B and Balser A W 2014 Elevated dissolved organic
706 carbon biodegradability from thawing and collapsing permafrost: Permafrost carbon
707 biodegradability *Journal of Geophysical Research: Biogeosciences* **119** 2049–63

708 Arrigo K R, Perovich D K, Pickart R S, Brown Z W, Dijken G L van, Lowry K E, Mills M M, Palmer M A, Balch
709 W M, Bahr F, Bates N R, Benitez-Nelson C, Bowler B, Brownlee E, Ehn J K, Frey K E, Garley R,
710 Laney S R, Lubelczyk L, Mathis J, Matsuoka A, Mitchell B G, Moore G W K, Ortega-Retuerta E, Pal
711 S, Polashenski C M, Reynolds R A, Schieber B, Sosik H M, Stephens M and Swift J H 2012 Massive
712 Phytoplankton Blooms Under Arctic Sea Ice *Science* **336** 1408–1408

713 Balshi M S, Mcguire A D, Duffy P, Flannigan M, Kicklighter D W and Melillo J 2009 Vulnerability of carbon
714 storage in North American boreal forests to wildfires during the 21st century *Global Change*
715 *Biology* **15** 1491–510

716 Barker A J, Douglas T A, Jacobson A D, McClelland J W, Ilgen A G, Khosh M S, Lehn G O and Trainor T P
717 2014 Late season mobilization of trace metals in two small Alaskan arctic watersheds as a proxy
718 for landscape scale permafrost active layer dynamics *Chemical Geology* **381** 180–93

719 Bernhardt E S, Blaszczak J R, Ficken C D, Fork M L, Kaiser K E and Seybold E C 2017 Control Points in
720 Ecosystems: Moving Beyond the Hot Spot Hot Moment Concept *Ecosystems* **20** 665–82

721 Berry Z C, Evaristo J, Moore G, Poca M, Steppe K, Verrot L, Asbjornsen H, Borma L S, Bretfeld M,
722 Hervé-Fernández P, Seyfried M, Schwendenmann L, Sinacore K, Wispelaere L D and McDonnell J
723 2018 The two water worlds hypothesis: Addressing multiple working hypotheses and proposing
724 a way forward *Ecohydrology* **11** e1843

725 Betts E F and Jones J B 2009 Impact of Wildfire on Stream Nutrient Chemistry and Ecosystem
726 Metabolism in Boreal Forest Catchments of Interior Alaska *Arctic, Antarctic, and Alpine Research*
727 **41** 407–17

728 Biskaborn B K, Smith S L, Noetzli J, Matthes H, Vieira G, Streletskiy D A, Schoeneich P, Romanovsky V E,
729 Lewkowicz A G, Abramov A, Allard M, Boike J, Cable W L, Christiansen H H, Delaloye R,
730 Diekmann B, Drozdov D, Etzelmüller B, Grosse G, Guglielmin M, Ingeman-Nielsen T, Isaksen K,
731 Ishikawa M, Johansson M, Johannsson H, Joo A, Kaverin D, Kholodov A, Konstantinov P, Kröger
732 T, Lambiel C, Lanckman J-P, Luo D, Malkova G, Meiklejohn I, Moskalenko N, Oliva M, Phillips M,
733 Ramos M, Sannel A B K, Sergeev D, Seybold C, Skryabin P, Vasiliev A, Wu Q, Yoshikawa K,
734 Zheleznyak M and Lantuit H 2019 Permafrost is warming at a global scale *Nature*
735 *Communications* **10** 264

736 Blume-Werry G, Wilson S D, Kreyling J and Milbau A 2016 The hidden season: growing season is 50%
737 longer below than above ground along an arctic elevation gradient *New Phytologist* **209** 978–86

738 Boelman N T, Rocha A V and Shaver G R 2011 Understanding burn severity sensing in Arctic tundra:
739 exploring vegetation indices, suboptimal assessment timing and the impact of increasing pixel
740 size *International Journal of Remote Sensing* **32** 7033–56

741 Bond-Lamberty B, Peckham S D, Ahl D E and Gower S T 2007 Fire as the dominant driver of central
742 Canadian boreal forest carbon balance *Nature* **450** 89–92

743 Bowden W B, Larouche J R, Pearce A R, Crosby B T, Krieger K, Flinn M B, Kampman J, Gooseff M N,
744 Godsey S E, Jones J B, Abbott B W, Jorgenson, M. T., Kling, G. W., Mack, M., Schuur, E. A. G.,
745 Baron, A. F., and Rastetter, E. B. 2012 An integrated assessment of the influences of upland
746 thermal-erosional features on landscape structure and function in the foothills of the Brooks
747 Range, Alaska *Tenth International Conference on Permafrost* vol 1 (Citeseer) pp 61–6 Online:
748 http://citeseerx.ist.psu.edu/viewdoc/download?doi=10.1.1.296.6775&rep=rep1&type=pdf

749 Bret-Harte M S, Mack M C, Shaver G R, Huebner D C, Johnston M, Mojica C A, Pizano C and Reiskind J A
750 2013 The response of Arctic vegetation and soils following an unusually severe tundra fire *Phil.*
751 *Trans. R. Soc. B* **368** 20120490

752 Brookshire E N J, Valett H M and Gerber S 2009 Maintenance of terrestrial nutrient loss signatures
753 during in-stream transport *Ecology* **90** 293–9

754 Buckeridge K M, Banerjee S, Siciliano S D and Grogan P 2013 The seasonal pattern of soil microbial
755 community structure in mesic low arctic tundra *Soil Biology and Biochemistry* **65** 338–47

756 Buckeridge K M and Grogan P 2010 Deepened snow increases late thaw biogeochemical pulses in mesic
757 low arctic tundra *Biogeochemistry* **101** 105–21

758 Buckeridge K M, Schaeffer S M and Schimel J P 2016 Vegetation Leachate During Arctic Thaw Enhances
759 Soil Microbial Phosphorus *Ecosystems* **19** 477–89

760 Burd K, Tank S E, Dion N, Quinton W L, Spence C, Tanentzap A J and Olefeldt D 2018 Seasonal shifts in
761 export of DOC and nutrients from burned and unburned peatland-rich catchments, Northwest
762 Territories, Canada *Hydrology and Earth System Sciences Discussions* 1–32

763 Bush R T, Berke M A and Jacobson A D 2017 Plant Water δD and δ18O of Tundra Species from West
764 Greenland *Arctic, Antarctic, and Alpine Research* **49** 341–58

765 Carey J C, Abbott B W and Rocha A V 2019 Plant Uptake Offsets Silica Release From a Large Arctic Tundra
766 Wildfire *Earth's Future* **7** 1044–57

767 Chen L, Liu L, Mao C, Qin S, Wang J, Liu F, Blagodatsky S, Yang G, Zhang Q, Zhang D, Yu J and Yang Y 2018
768 Nitrogen availability regulates topsoil carbon dynamics after permafrost thaw by altering
769 microbial metabolic efficiency *Nat Commun* **9** 1–11

770 Coch C, Juhls B, Lamoureux S F, Lafrenière M J, Fritz M, Heim B and Lantuit H 2019 Comparisons of
771 dissolved organic matter and its optical characteristics in small low and high Arctic catchments
772 *Biogeosciences* **16** 4535–53

773 Cory R M, Miller M P, McKnight D M, Guerard J J and Miller P L 2010 Effect of instrument-specific
774 response on the analysis of fulvic acid fluorescence spectra *Limnology and Oceanography:*
775 *Methods* **8** 67–78

776 Craine J M, Morrow C and Fierer N 2007 Microbial Nitrogen Limitation Increases Decomposition *Ecology*
777 **88** 2105–13

778 Creed I F, Bergström A-K, Trick C G, Grimm N B, Hessen D O, Karlsson J, Kidd K A, Kritzberg E, McKnight D
779 M, Freeman E C, Senar O E, Andersson A, Ask J, Berggren M, Cherif M, Giesler R, Hotchkiss E R,
780 Kortelainen P, Palta M M, Vrede T and Weyhenmeyer G A 2018 Global change-driven effects on
781 dissolved organic matter composition: Implications for food webs of northern lakes *Global*
782 *Change Biology* **24** 3692–714

783 Crump B C, Amaral-Zettler L A and Kling G W 2012 Microbial diversity in arctic freshwaters is structured
784 by inoculation of microbes from soils *ISME J* **6** 1629–39

785 Darrouzet-Nardi A, Steltzer H, Sullivan P F, Segal A, Koltz A M, Livensperger C, Schimel J P and Weintraub
786 M N 2019 Limited effects of early snowmelt on plants, decomposers, and soil nutrients in Arctic
787 tundra soils *Ecology and Evolution* **9** 1820–44

788 DeMarco J, Mack M C and Bret-Harte M S 2011 The Effects of Snow, Soil Microenvironment, and Soil
789 Organic Matter Quality on N Availability in Three Alaskan Arctic Plant Communities *Ecosystems*
790 **14** 804–17

791 Douglas T A, Turetsky M R and Koven C D 2020 Increased rainfall stimulates permafrost thaw across a
792 variety of Interior Alaskan boreal ecosystems *npj Climate and Atmospheric Science* **3** 1–7

793 Drake T W, Tank S E, Zhulidov A V, Holmes R M, Gurtovaya T and Spencer R G M 2018 Increasing
794 Alkalinity Export from Large Russian Arctic Rivers *Environ. Sci. Technol.* **52** 8302–8

795 Dupas R, Minaudo C and Abbott B W 2019 Stability of spatial patterns in water chemistry across
796 temperate ecoregions *Environ. Res. Lett.* **14** 074015

797 Ewing S A, O'Donnell J A, Aiken G R, Butler K, Butman D, Windham-Myers L and Kanevskiy M Z 2015
798 Long-term anoxia and release of ancient, labile carbon upon thaw of Pleistocene permafrost
799 *Geophys. Res. Lett.* **42** 2015GL066296

800 Fellman J B, Spencer R G M, Hernes P J, Edwards R T, D'Amore D V and Hood E 2010 The impact of
801 glacier runoff on the biodegradability and biochemical composition of terrigenous dissolved
802 organic matter in near-shore marine ecosystems *Marine Chemistry* **121** 112–22

803 Fisher R A, Wieder W R, Sanderson B M, Koven C D, Oleson K W, Xu C, Fisher J B, Shi M, Walker A P and
804 Lawrence D M 2019 Parametric Controls on Vegetation Responses to Biogeochemical Forcing in
805 the CLM5 *Journal of Advances in Modeling Earth Systems* **11** 2879–95

806 Fisher S G, Grimm N B, Martí E, Holmes R M and Jones Jr J B 1998 Material spiraling in stream corridors:
807 a telescoping ecosystem model *Ecosystems* **1** 19–34

808 Frei R J, Abbott B W, Dupas R, Gu S, Gruau G, Thomas Z, Kolbe T, Aquilina L, Labasque T, Laverman A,
809 Fovet O, Moatar F and Pinay G 2020 Predicting Nutrient Incontinence in the Anthropocene at
810 Watershed Scales *Front. Environ. Sci.* **7** Online:
811 https://www.frontiersin.org/articles/10.3389/fenvs.2019.00200/full?&utm_source=Email_to_a
812 uthors_&utm_medium=Email&utm_content=T1_11.5e1_author&utm_campaign=Email_publica
813 tion&field=&journalName=Frontiers_in_Environmental_Science&id=480162

814 Frey K E and McClelland J W 2009 Impacts of permafrost degradation on arctic river biogeochemistry
815 *Hydrological Processes* **23** 169–82

816 Frey K E, McClelland J W, Holmes R M and Smith L C 2007 Impacts of climate warming and permafrost
817 thaw on the riverine transport of nitrogen and phosphorus to the Kara Sea *Journal of*
818 *Geophysical Research* **112** Online: http://doi.wiley.com/10.1029/2006JG000369

819 Frost G V, Epstein H E, Walker D A, Matyshak G and Ermokhina K 2013 Patterned-ground facilitates
820 shrub expansion in Low Arctic tundra *Environmental Research Letters* **8** 015035

821 Gabor R S, Baker A, McKnight D M and Miller M P 2014 Fluorescence Indices and Their Interpretation
822 *Aquatic Organic Matter Fluorescence* Cambridge Environmental Chemistry Series ed A Baker, D
823 M Reynolds, J Lead, P G Coble and R G M Spencer (Cambridge: Cambridge University Press) pp
824 303–38 Online: https://www.cambridge.org/core/books/aquatic-organic-matter-
825 fluorescence/fluorescence-indices-and-their-
826 interpretation/2BB8ADC43278DE03EC24EA2F11B3E94C

827 Gabor R S, Burns M A, Lee R H, Elg J B, Kemper C J, Barnard H R and McKnight D M 2015 Influence of
828 Leaching Solution and Catchment Location on the Fluorescence of Water-Soluble Organic
829 Matter *Environmental Science & Technology* **49** 4425–32

830 Gaglioti B V, Mann D H, Jones B M, Pohlman J W, Kunz M L and Wooller M J 2014 Radiocarbon age-
831 offsets in an arctic lake reveal the long-term response of permafrost carbon to climate change
832 *Journal of Geophysical Research: Biogeosciences* **119** 1630–51

833 Harms T K, Abbott B W and Jones J B 2014 Thermo-erosion gullies increase nitrogen available for
834 hydrologic export *Biogeochemistry* **117** 299–311

Harms T K and Godsey S E 2017 *Water isotopes of precipitation, surface, and soil waters of the Kuparuk River Basin. Arctic Data Center.* (Arctic Data Center) Online: https://arcticdata.io/catalog/view/668ee3cc-f1f8-43ca-b977-339a8eb0aea5

Harms T K and Jones J B 2012 Thaw depth determines reaction and transport of inorganic nitrogen in valley bottom permafrost soils *Glob Change Biol* **18** 2958–68

Hewitt R E, Bennett A P, Breen A L, Hollingsworth T N, Taylor D L, Chapin F S and Rupp T S 2015 Getting to the root of the matter: landscape implications of plant-fungal interactions for tree migration in Alaska *Landscape Ecology* Online: http://link.springer.com/10.1007/s10980-015-0306-1

Higuera P E, Chipman M L, Barnes J L, Urban M A and Hu F S 2011 Variability of tundra fire regimes in Arctic Alaska: millennial-scale patterns and ecological implications *Ecological Applications* **21** 3211–26

Hoffman F M, Koven C D, Keppel-Aleks G, Lawrence D M, Riley W J, Randerson J T, Ahlström A, Abramowitz G, Baldocchi D D, Best M J, Bond-Lamberty B, De Kauwe M G, Denning A S, Desai A R, Eyring V, Fisher J B, Fisher R A, Gleckler P J, Huang M, Hugelius G, Jain A K, Kiang N Y, Kim H, Koster R D, Kumar S V, Li H, Luo Y, Mao J, McDowell N G, Mishra U, Moorcroft P R, Pau G S H, Ricciuto D M, Schaefer K, Schwalm C R, Serbin S P, Shevliakova E, Slater A G, Tang J, Williams M, Xia J, Xu C, Joseph R and Koch D 2017 *2016 International Land Model Benchmarking (ILAMB) Workshop Report* Online: http://www.osti.gov/servlets/purl/1330803/

Högberg M N, Briones M J I, Keel S G, Metcalfe D B, Campbell C, Midwood A J, Thornton B, Hurry V, Linder S, Näsholm T and Högberg P 2010 Quantification of effects of season and nitrogen supply on tree below-ground carbon transfer to ectomycorrhizal fungi and other soil organisms in a boreal pine forest *New Phytologist* **187** 485–93

Holloway J E, Lewkowicz A G, Douglas T A, Li X, Turetsky M R, Baltzer J L and Jin H 2020 Impact of wildfire on permafrost landscapes: A review of recent advances and future prospects *Permafrost and Periglacial Processes* **31** 371–82

Holmes R M, McClelland J W, Peterson B J, Tank S E, Bulygina E, Eglinton T I, Gordeev V V, Gurtovaya T Y, Raymond P A, Repeta D J, Staples R, Striegl R G, Zhulidov A V and Zimov S A 2012 Seasonal and Annual Fluxes of Nutrients and Organic Matter from Large Rivers to the Arctic Ocean and Surrounding Seas *Estuaries and Coasts* **35** 369–82

Hu F S, Higuera P E, Duffy P, Chipman M L, Rocha A V, Young A M, Kelly R and Dietze M C 2015 Arctic tundra fires: natural variability and responses to climate change *Frontiers in Ecology and the Environment* **13** 369–77

Hu F S, Higuera P E, Walsh J E, Chapman W L, Duffy P A, Brubaker L B and Chipman M L 2010 Tundra burning in Alaska: Linkages to climatic change and sea ice retreat *Journal of Geophysical Research: Biogeosciences* **115** Online: https://agupubs.onlinelibrary.wiley.com/doi/abs/10.1029/2009JG001270

Hugelius G 2012 Spatial upscaling using thematic maps: An analysis of uncertainties in permafrost soil carbon estimates *Global Biogeochemical Cycles* **26** n/a-n/a

Hurrell J W, Holland M M, Gent P R, Ghan S, Kay J E, Kushner P J, Lamarque J-F, Large W G, Lawrence D, Lindsay K, Lipscomb W H, Long M C, Mahowald N, Marsh D R, Neale R B, Rasch P, Vavrus S, Vertenstein M, Bader D, Collins W D, Hack J J, Kiehl J and Marshall S 2013 The Community Earth System Model: A Framework for Collaborative Research *Bull. Amer. Meteor. Soc.* **94** 1339–60

Iwahana G, Harada K, Uchida M, Tsuyuzaki S, Saito K, Narita K, Kushida K and Hinzman L D 2016 Geomorphological and geochemistry changes in permafrost after the 2002 tundra wildfire in Kougarok, Seward Peninsula, Alaska *J. Geophys. Res. Earth Surf.* **121** 2016JF003921

Jandt R R, Miller E A, Yokel D A, Bret-Harte M S, Kolden C A and Mack M C 2012 *Findings of Anaktuvuk River Fire Recovery Study, 2007-2011* Online: https://www.sciencebase.gov/catalog/item/5a3946c7e4b0d05ee8b407a0

Jiang Y, Rastetter E B, Rocha A V, Pearce A R, Kwiatkowski B L and Shaver G R 2015a Modeling carbon–nutrient interactions during the early recovery of tundra after fire *Ecological Applications* **25** 1640–52

Jiang Y, Rastetter E B, Shaver G R, Rocha A V, Zhuang Q and Kwiatkowski B L 2017 Modeling long-term changes in tundra carbon balance following wildfire, climate change, and potential nutrient addition *Ecological Applications* **27** 105–17

Jiang Y, Rocha A V, O'Donnell J A, Drysdale J A, Rastetter E B, Shaver G R and Zhuang Q 2014 Contrasting soil thermal responses to fire in Alaskan tundra and boreal forest *Journal of Geophysical Research: Earth Surface* **120** 363–78

Jiang Y, Rocha A V, Rastetter E B, Shaver G R, Mishra U, Zhuang Q and Kwiatkowski B L 2015b C–N–P interactions control climate driven changes in regional patterns of C storage on the North Slope of Alaska *Landscape Ecology* Online: http://link.springer.com/10.1007/s10980-015-0266-5

Jones B M, Breen A L, Gaglioti B V, Mann D H, Rocha A V, Grosse G, Arp C D, Kunz M L and Walker D A 2013 Identification of unrecognized tundra fire events on the north slope of Alaska *Journal of Geophysical Research: Biogeosciences* **118** 1334–44

Jones B M, Grosse G, Arp C D, Miller E, Liu L, Hayes D J and Larsen C F 2015 Recent Arctic tundra fire initiates widespread thermokarst development *Scientific Reports* **5** 15865

Jones B M, Kolden C A, Jandt R, Abatzoglou J T, Urban F and Arp C D 2009 Fire Behavior, Weather, and Burn Severity of the 2007 Anaktuvuk River Tundra Fire, North Slope, Alaska *Arctic, Antarctic, and Alpine Research* **41** 309–16

Jones J B, Petrone K C, Finlay J C, Hinzman L D and Bolton W R 2005 Nitrogen loss from watersheds of interior Alaska underlain with discontinuous permafrost *Geophys. Res. Lett.* **32** L02401

Jorgenson M T, Harden J, Kanevskiy M, O'Donnell J, Wickland K, Ewing S, Manies K, Zhuang Q, Shur Y, Striegl R and Koch J 2013 Reorganization of vegetation, hydrology and soil carbon after permafrost degradation across heterogeneous boreal landscapes *Environmental Research Letters* **8** 035017

909 Jorgenson M T and Osterkamp T E 2005 Response of boreal ecosystems to varying modes of permafrost
910 degradation *Canadian Journal of Forest Research* **35** 2100–11

911 Kawahigashi M, Kaiser K, Rodionov A and Guggenberger G 2006 Sorption of dissolved organic matter by
912 mineral soils of the Siberian forest tundra *Global Change Biology* **12** 1868–77

913 Kawahigashi M, Prokushkin A and Sumida H 2011 Effect of fire on solute release from organic horizons
914 under larch forest in Central Siberian permafrost terrain *Geoderma* **166** 171–80

915 Kelleher C, Ward A, Knapp J L A, Blaen P J, Kurz M J, Drummond J D, Zarnetske J P, Hannah D M,
916 Mendoza-Lera C, Schmadel N M, Datry T, Lewandowski J, Milner A M and Krause S 2019
917 Exploring Tracer Information and Model Framework Trade-Offs to Improve Estimation of Stream
918 Transient Storage Processes *Water Resources Research* **55** 3481–501

919 Keller K, Blum J D and Kling G W 2010 Stream geochemistry as an indicator of increasing permafrost
920 thaw depth in an arctic watershed *Chemical Geology* **273** 76–81

921 Kellerman A M, Guillemette F, Podgorski D C, Aiken G R, Butler K D and Spencer R G M 2018 Unifying
922 Concepts Linking Dissolved Organic Matter Composition to Persistence in Aquatic Ecosystems
923 *Environ. Sci. Technol.* **52** 2538–48

924 Kendrick M R, Huryn A D, Bowden W B, Deegan L A, Findlay R H, Hershey A E, Peterson B J, Beneš J P and
925 Schuett E B 2018 Linking permafrost thaw to shifting biogeochemistry and food web resources
926 in an arctic river *Global Change Biology* **24** 5738–50

927 Keuper F, Dorrepaal E, Bodegom P M van, Logtestijn R van, Venhuizen G, Hal J van and Aerts R 2017
928 Experimentally increased nutrient availability at the permafrost thaw front selectively enhances
929 biomass production of deep-rooting subarctic peatland species *Global Change Biology* **23** 4257–
930 66

931 Keuper F, Wild B, Kummu M, Beer C, Blume-Werry G, Fontaine S, Gavazov K, Gentsch N, Guggenberger
932 G, Hugelius G, Jalava M, Koven C, Krab E J, Kuhry P, Monteux S, Richter A, Shahzad T, Weedon J T
933 and Dorrepaal E 2020 Carbon loss from northern circumpolar permafrost soils amplified by
934 rhizosphere priming *Nature Geoscience* 1–6

935 Kicklighter D W, Hayes D J, McClelland J W, Peterson B J, McGuire A D and Melillo J M 2013 Insights and
936 issues with simulating terrestrial DOC loading of Arctic river networks *Ecological Applications* **23**
937 1817–36

938 Kim J-S, Kug J-S, Jeong S-J, Park H and Schaepman-Strub G 2020 Extensive fires in southeastern Siberian
939 permafrost linked to preceding Arctic Oscillation *Science Advances* **6** eaax3308

940 King T V, Neilson B T, Overbeck L D and Kane D L 2016 Water temperature controls in low arctic rivers
941 *Water Resources Research* **52** 4358–76

942 King T V, Neilson B T and Rasmussen M T 2018 Estimating Discharge in Low-Order Rivers With High-
943 Resolution Aerial Imagery *Water Resources Research* **54** 863–78

944 Kirdyanov A, Saurer M, Siegwolf R, Knorre A A, Prokushkin A, Churakova (Sidorova) O V, Fonti M V and
945 Buentgen U 2020 Long-term ecological consequences of forest fires in the continuous
946 permafrost zone of Siberia *Environ. Res. Lett.* Online: http://iopscience.iop.org/10.1088/1748-
947 9326/ab7469

948 Kling G W, Kipphut G W, Miller M M and O'Brien W JohN 2000 Integration of lakes and streams in a
949 landscape perspective: the importance of material processing on spatial patterns and temporal
950 coherence *Freshwater Biology* **43** 477–97

951 Kokelj S V and Jorgenson M T 2013 Advances in Thermokarst Research: Recent Advances in Research
952 Investigating Thermokarst Processes *Permafrost and Periglacial Processes* **24** 108–19

953 Kolden C A and Rogan J 2013 Mapping Wildfire Burn Severity in the Arctic Tundra from Downsampled
954 MODIS Data *Arctic, Antarctic, and Alpine Research* **45** 64–76

955 Kou D, Yang G, Li F, Feng X, Zhang D, Mao C, Zhang Q, Peng Y, Ji C, Zhu Q, Fang Y, Liu X, Xu-Ri, Li S, Deng
956 J, Zheng X, Fang J and Yang Y 2020 Progressive nitrogen limitation across the Tibetan alpine
957 permafrost region *Nature Communications* **11** 3331

958 Landhausser S M and Wein R W 1993 Postfire Vegetation Recovery and Tree Establishment at the Arctic
959 Treeline: Climate-Change-Vegetation-Response Hypotheses *Journal of Ecology* **81** 665–72

960 Larouche J R, Abbott B W, Bowden W B and Jones J B 2015 The role of watershed characteristics,
961 permafrost thaw, and wildfire on dissolved organic carbon biodegradability and water chemistry
962 in Arctic headwater streams *Biogeosciences* **12** 4221–33

963 Laudon H, Tetzlaff D, Soulsby C, Carey S, Seibert J, Buttle J, Shanley J, McDonnell J J and McGuire K 2013
964 Change in winter climate will affect dissolved organic carbon and water fluxes in mid-to-high
965 latitude catchments *Hydrol. Process.* **27** 700–9

966 Lawrence D M, Koven C D, Swenson S C, Riley W J and Slater A G 2015 Permafrost thaw and resulting soil
967 moisture changes regulate projected high-latitude CO2 and CH4 emissions *Environmental*
968 *Research Letters* **10** 094011

969 Lawrence D M, Oleson K W, Flanner M G, Thornton P E, Swenson S C, Lawrence P J, Zeng X, Yang Z-L,
970 Levis S, Sakaguchi K, Bonan G B and Slater A G 2011 Parameterization improvements and
971 functional and structural advances in Version 4 of the Community Land Model *J. Adv. Model.*
972 *Earth Syst.* **3** M03001

973 Lehn G O, Jacobson A D, Douglas T A, McClelland J W, Barker A J and Khosh M S 2017 Constraining
974 seasonal active layer dynamics and chemical weathering reactions occurring in North Slope
975 Alaskan watersheds with major ion and isotope (δ 34 S SO4 , δ 13 C DIC , 87 Sr/ 86 Sr, δ 44/40
976 Ca, and δ 44/42 Ca) measurements *Geochimica et Cosmochimica Acta* **217** 399–420

977 Liu L, Jafarov E E, Schaefer K M, Jones B M, Zebker H A, Williams C A, Rogan J and Zhang T 2014 InSAR
978 detects increase in surface subsidence caused by an Arctic tundra fire *Geophysical Research*
979 *Letters* **41** 3906–13

Loranty M M, Abbott B W, Blok D, Douglas T A, Epstein H E, Forbes B C, Jones B M, Kholodov A L, Kropp H, Malhotra A, Mamet S D, Myers-Smith I H, Natali S M, O'Donnell J A, Phoenix G K, Rocha A V, Sonnentag O, Tape K D and Walker D A 2018 Reviews and syntheses: Changing ecosystem influences on soil thermal regimes in northern high-latitude permafrost regions *Biogeosciences* **15** 5287–313

Loranty M M, Liberman-Cribbin W, Berner L T, Natali S M, Goetz S J, Alexander H D and Kholodov A L 2016 Spatial variation in vegetation productivity trends, fire disturbance, and soil carbon across arctic-boreal permafrost ecosystems *Environmental Research Letters* **11** 095008

Lovett G M, Goodale C L, Ollinger S V, Fuss C B, Ouimette A P and Likens G E 2018 Nutrient retention during ecosystem succession: a revised conceptual model *Frontiers in Ecology and the Environment* **16** 532–8

Ludwig S M, Alexander H D, Kielland K, Mann P J, Natali S M and Ruess R W 2018 Fire severity effects on soil carbon and nutrients and microbial processes in a Siberian larch forest *Glob Change Biol* **24** 5841–52

Lyon S W, Nathanson M, Spans A, Grabs T, Laudon H, Temnerud J, Bishop K H and Seibert J 2012 Specific discharge variability in a boreal landscape *Water Resour. Res.* **48** W08506

Mack M C, Bret-Harte M S, Hollingsworth T N, Jandt R R, Schuur E A G, Shaver G R and Verbyla D L 2011 Carbon loss from an unprecedented Arctic tundra wildfire *Nature* **475** 489–92

Mack M C, Schuur E A G, Bret-Harte M S, Shaver G R and Chapin F S 2004 Ecosystem carbon storage in arctic tundra reduced by long-term nutrient fertilization *Nature* **431** 440–3

Mack M C, Treseder K K, Manies K L, Harden J W, Schuur E A G, Vogel J G, Randerson J T and Chapin F S 2008 Recovery of Aboveground Plant Biomass and Productivity After Fire in Mesic and Dry Black Spruce Forests of Interior Alaska *Ecosystems* **11** 209–25

MacLean R, Oswood M W, Irons J G and McDowell W H 1999 The effect of permafrost on stream biogeochemistry: A case study of two streams in the Alaskan (U.S.A.) taiga *Biogeochemistry* **47** 239–67

Malone E T, Abbott B W, Klaar M J, Kidd C, Sebilo M, Milner A M and Pinay G 2018 Decline in Ecosystem δ13C and Mid-Successional Nitrogen Loss in a Two-Century Postglacial Chronosequence *Ecosystems* **21** 1659–75

Mann P J, Spencer R G M, Hernes P J, Six J, Aiken G R, Tank S E, McClelland J W, Butler K D, Dyda R Y and Holmes R M 2016 Pan-Arctic Trends in Terrestrial Dissolved Organic Matter from Optical Measurements *Front. Earth Sci.* **4** Online: http://journal.frontiersin.org/article/10.3389/feart.2016.00025/abstract

McClelland J W, Holmes R M, Dunton K H and Macdonald R W 2012 The Arctic Ocean Estuary *Estuaries and Coasts* **35** 353–68

1015 McClelland J W, Stieglitz M, Pan F, Holmes R M and Peterson B J 2007 Recent changes in nitrate and
1016 dissolved organic carbon export from the upper Kuparuk River, North Slope, Alaska *Journal of*
1017 *Geophysical Research* **112** Online: http://doi.wiley.com/10.1029/2006JG000371

1018 McClelland J W, Townsend-Small A, Holmes R M, Pan F, Stieglitz M, Khosh M and Peterson B J 2014 River
1019 export of nutrients and organic matter from the North Slope of Alaska to the Beaufort Sea
1020 *Water Resources Research* **50** 1823–39

1021 McGuire A D, Lawrence D M, Koven C, Clein J S, Burke E, Chen G, Jafarov E, MacDougall A H, Marchenko
1022 S, Nicolsky D, Peng S, Rinke A, Ciais P, Gouttevin I, Hayes D J, Ji D, Krinner G, Moore J C,
1023 Romanovsky V, Schädel C, Schaefer K, Schuur E A G and Zhuang Q 2018 Dependence of the
1024 evolution of carbon dynamics in the northern permafrost region on the trajectory of climate
1025 change *PNAS* **115** 3882–7

1026 McGuire K J, Torgersen C E, Likens G E, Buso D C, Lowe W H and Bailey S W 2014 Network analysis
1027 reveals multiscale controls on streamwater chemistry *PNAS* **111** 7030–5

1028 McKnight D M, Boyer E W, Westerhoff P K, Doran P T, Kulbe T and Andersen D T 2001
1029 Spectrofluorometric characterization of dissolved organic matter for indication of precursor
1030 organic material and aromaticity *Limnol. Oceanogr.* **46** 38–48

1031 McLaren J R, Darrouzet-Nardi A, Weintraub M N and Gough L 2017 Seasonal patterns of soil nitrogen
1032 availability in moist acidic tundra *Arctic Science* Online:
1033 https://cdnsciencepub.com/doi/abs/10.1139/AS-2017-0014

1034 Melle C, Wallenstein M, Darrouzet-Nardi A and Weintraub M N 2015 Microbial activity is not always
1035 limited by nitrogen in Arctic tundra soils *Soil Biology and Biochemistry* **90** 52–61

1036 Metcalfe D B, Hermans T D G, Ahlstrand J, Becker M, Berggren M, Björk R G, Björkman M P, Blok D,
1037 Chaudhary N, Chisholm C, Classen A T, Hasselquist N J, Jonsson M, Kristensen J A, Kumordzi B B,
1038 Lee H, Mayor J R, Prevéy J, Pantazatou K, Rousk J, Sponseller R A, Sundqvist M K, Tang J, Uddling
1039 J, Wallin G, Zhang W, Ahlström A, Tenenbaum D E and Abdi A M 2018 Patchy field sampling
1040 biases understanding of climate change impacts across the Arctic *Nature Ecology & Evolution* 1

1041 Minaudo C, Dupas R, Gascuel-Odoux C, Fovet O, Mellander P-E, Jordan P, Shore M and Moatar F 2017
1042 Nonlinear empirical modeling to estimate phosphorus exports using continuous records of
1043 turbidity and discharge: P EXPORTS FROM TURBIDITY AND DISCHARGE *Water Resources*
1044 *Research* **53** 7590–606

1045 Mollenhauer G, Winterfeld M, Hefter J, Grotheer H, Kattein L and Ransby D 2019 No evidence for 20th
1046 century acceleration in fossil carbon supply to the ocean from thawing permafrost in the Lena
1047 River catchment *EPIC3Goldschmidt Conference, Barcelona, 2019-08-18-2019-08-23* Goldschmidt
1048 Conference (Barcelona) Online: https://epic.awi.de/id/eprint/50144/

1049 Mu C C, Abbott B W, Wu X D, Zhao Q, Wang H J, Su H, Wang S F, Gao T G, Guo H, Peng X Q and Zhang T J
1050 2017 Thaw Depth Determines Dissolved Organic Carbon Concentration and Biodegradability on
1051 the Northern Qinghai-Tibetan Plateau *Geophys. Res. Lett.* 2017GL075067

Myers-Smith I H, Elmendorf S C, Beck P S A, Wilmking M, Hallinger M, Blok D, Tape K D, Rayback S A, Macias-Fauria M, Forbes B C, Speed J D M, Boulanger-Lapointe N, Rixen C, Lévesque E, Schmidt N M, Baittinger C, Trant A J, Hermanutz L, Collier L S, Dawes M A, Lantz T C, Weijers S, Jørgensen R H, Buchwal A, Buras A, Naito A T, Ravolainen V, Schaepman-Strub G, Wheeler J A, Wipf S, Guay K C, Hik D S and Vellend M 2015 Climate sensitivity of shrub growth across the tundra biome *Nature Climate Change* **5** nclimate2697

Myers-Smith I H, Forbes B C, Wilmking M, Hallinger M, Lantz T, Blok D, Tape K D, Macias-Fauria M, Sass-Klaassen U, Lévesque E, Boudreau S, Ropars P, Hermanutz L, Trant A, Collier L S, Weijers S, Rozema J, Rayback S A, Schmidt N M, Schaepman-Strub G, Wipf S, Rixen C, Ménard C B, Venn S, Goetz S, Andreu-Hayles L, Elmendorf S, Ravolainen V, Welker J, Grogan P, Epstein H E and Hik D S 2011 Shrub expansion in tundra ecosystems: dynamics, impacts and research priorities *Environmental Research Letters* **6** 045509

Neilson B T, Cardenas M B, O'Connor M T, Rasmussen M T, King T V and Kling G W 2018 Groundwater Flow and Exchange Across the Land Surface Explain Carbon Export Patterns in Continuous Permafrost Watersheds *Geophysical Research Letters* **45** 7596–605

Neumann R B, Moorberg C J, Lundquist J D, Turner J C, Waldrop M P, McFarland J W, Euskirchen E S, Edgar C W and Turetsky M R 2019 Warming Effects of Spring Rainfall Increase Methane Emissions From Thawing Permafrost *Geophysical Research Letters* **46** 1393–401

Oberbauer S F, Sionit N, Hastings S J and Oechel W C 1986 Effects of CO2 enrichment and nutrition on growth, photosynthesis, and nutrient concentration of Alaskan tundra plant species *Canadian Journal of Botany* **64** 2993–8

O'Donnell J A, Aiken G R, Butler K D, Guillemette F, Podgorski D C and Spencer R G M 2016a DOM composition and transformation in boreal forest soils: The effects of temperature and organic-horizon decomposition state *J. Geophys. Res. Biogeosci.* **121** 2016JG003431

O'Donnell J A, Aiken G R, Swanson D K, Panda S, Butler K D and Baltensperger A P 2016b Dissolved organic matter composition of Arctic rivers: Linking permafrost and parent material to riverine carbon *Global Biogeochem. Cycles* 2016GB005482

O'Donnell J A, Harden J W, Manies K L, Jorgenson M T, Kanevskiy M and Xu X 2013 *Soil data from fire and permafrost-thaw chronosequences in upland Picea mariana stands near Hess Creek and Tok, interior Alaska* vol 2013–1045 (Reston, VA: U.S. Geological Survey) Online: http://pubs.er.usgs.gov/publication/ofr20131045

Olefeldt D, Goswami S, Grosse G, Hayes D, Hugelius G, Kuhry P, McGuire A D, Romanovsky V E, Sannel A B K, Schuur E A G and Turetsky M R 2016 Circumpolar distribution and carbon storage of thermokarst landscapes *Nature Communications* **7** 13043

Parham L M, Prokushkin A S, Pokrovsky O S, Titov S V, Grekova E, Shirokova L S and McDowell W H 2013 Permafrost and fire as regulators of stream chemistry in basins of the Central Siberian Plateau *Biogeochemistry* **116** 55–68

1089 Pearce A R, Rastetter E B, Kwiatkowski B L, Bowden W B, Mack M C and Jiang Y 2014 Recovery of arctic
1090 tundra from thermal erosion disturbance is constrained by nutrient accumulation: a modeling
1091 analysis *Ecological Applications* Online: http://www.esajournals.org/doi/abs/10.1890/14-1323.1

1092 Petrone K C, Jones J B, Hinzman L D and Boone R D 2006 Seasonal export of carbon, nitrogen, and major
1093 solutes from Alaskan catchments with discontinuous permafrost *Journal of Geophysical*
1094 *Research* **111** Online: http://doi.wiley.com/10.1029/2005JG000055

1095 Pinay G, Peiffer S, De Dreuzy J-R, Krause S, Hannah D M, Fleckenstein J H, Sebilo M, Bishop K and Hubert-
1096 Moy L 2015 Upscaling Nitrogen Removal Capacity from Local Hotspots to Low Stream Orders'
1097 Drainage Basins *Ecosystems* **18** 1101–20

1098 Porter C, Morin P, Howat I, Noh M-J, Bates B, Peterman K, Keesey S, Schlenk M, Gardiner J, Tomko K,
1099 Willis M, Kelleher C, Cloutier M, Husby E, Foga S, Nakamura H, Platson M, Wethington M,
1100 Williamson C, Bauer G, Enos J, Arnold G, Kramer W, Becker P, Doshi A, D'Souza C, Cummens P,
1101 Laurier F and Bojesen M 2018 ArcticDEM Online:
1102 https://dataverse.harvard.edu/citation?persistentId=doi:10.7910/DVN/OHHUKH

1103 R Core Team 2018 *R: A Language and Environment for Statistical Computing* (Vienna, Austria: R
1104 Foundation for Statistical Computing) Online: https://www.R-project.org/

1105 Racine C, Jandt R, Meyers C and Dennis J 2004 Tundra Fire and Vegetation Change along a Hillslope on
1106 the Seward Peninsula, Alaska, U.S.A *Arctic, Antarctic, and Alpine Research* **36** 1–10

1107 Rastetter E B, Kling G W, Shaver G R, Crump B C, Gough L and Griffin K L 2020 Ecosystem Recovery from
1108 Disturbance is Constrained by N Cycle Openness, Vegetation-Soil N Distribution, Form of N
1109 Losses, and the Balance Between Vegetation and Soil-Microbial Processes *Ecosystems* Online:
1110 https://doi.org/10.1007/s10021-020-00542-3

1111 Raymond P A, McClelland J W, Holmes R M, Zhulidov A V, Mull K, Peterson B J, Striegl R G, Aiken G R and
1112 Gurtovaya T Y 2007 Flux and age of dissolved organic carbon exported to the Arctic Ocean: A
1113 carbon isotopic study of the five largest arctic rivers *Global Biogeochem. Cycles* **21** GB4011

1114 Rey D M, Walvoord M A, Minsley B J, Ebel B A, Voss C I and Singha K 2020 Wildfire initiated talik
1115 development exceeds current thaw projections: Observations and models from Alaska's
1116 continuous permafrost zone *Geophysical Research Letters* e2020GL087565

1117 Reyes F R and Lougheed V L 2015 Rapid Nutrient Release from Permafrost Thaw in Arctic Aquatic
1118 Ecosystems *Arctic, Antarctic, and Alpine Research* **47** 35–48

1119 Rhoades C, Oskarsson H, Binkley D and Stottlemyer B 2001 Alder (Alnus crispa) effects on soils in
1120 ecosystems of the Agashashok River valley, northwest Alaska *Écoscience* **8** 89–95

1121 Rocha A V, Loranty M M, Higuera P E, Mack M C, Hu F S, Jones B M, Breen A L, Rastetter E B, Goetz S J
1122 and Shaver G R 2012 The footprint of Alaskan tundra fires during the past half-century:
1123 implications for surface properties and radiative forcing *Environ. Res. Lett.* **7** 044039

1124 Rocha A V and Shaver G R 2011a Burn severity influences postfire CO2 exchange in arctic tundra
1125 *Ecological Applications* **21** 477–89

1126 Rocha A V and Shaver G R 2011b Postfire energy exchange in arctic tundra: the importance and climatic
1127 implications of burn severity *Global Change Biology* **17** 2831–41

1128 Rodríguez-Cardona B M, Coble A A, Wymore A S, Kolosov R, Podgorski D C, Zito P, Spencer R G M,
1129 Prokushkin A S and McDowell W H 2020 Wildfires lead to decreased carbon and increased
1130 nitrogen concentrations in upland arctic streams *Scientific Reports* **10** 8722

1131 Ruess R W, Anderson M D, McFarland J M, Kielland K, Olson K and Taylor D L 2013 Ecosystem-level
1132 consequences of symbiont partnerships in an N-fixing shrub from interior Alaskan floodplains
1133 *Ecological Monographs* **83** 177–94

1134 Salmon V G, Schädel C, Bracho R, Pegoraro E, Celis G, Mauritz M, Mack M C and Schuur E A G 2018
1135 Adding Depth to Our Understanding of Nitrogen Dynamics in Permafrost Soils *Journal of*
1136 *Geophysical Research: Biogeosciences* **123** 2497–512

1137 Schuur E A G, McGuire A D, Schädel C, Grosse G, Harden J W, Hayes D J, Hugelius G, Koven C D, Kuhry P,
1138 Lawrence D M, Natali S M, Olefeldt D, Romanovsky V E, Schaefer K, Turetsky M R, Treat C C and
1139 Vonk J E 2015 Climate change and the permafrost carbon feedback *Nature* **520** 171–9

1140 Shogren A J, Zarnetske J P, Abbott B W, Iannucci F and Bowden W B 2020 We cannot shrug off the
1141 shoulder seasons: Addressing knowledge and data gaps in an Arctic Headwater *Environ. Res.*
1142 *Lett.* Online: https://doi.org/10.1088%2F1748-9326%2Fab9d3c

1143 Shogren A J, Zarnetske J P, Abbott B W, Iannucci F, Frei R J, Griffin N A and Bowden W B 2019 Revealing
1144 biogeochemical signatures of Arctic landscapes with river chemistry *Sci Rep* **9** 1–11

1145 Shur Y L and Jorgenson M T 2007 Patterns of permafrost formation and degradation in relation to
1146 climate and ecosystems *Permafrost and Periglacial Processes* **18** 7–19

1147 Sigman D M, Casciotti K L, Andreani M, Barford C, Galanter M and Böhlke J K 2001 A Bacterial Method
1148 for the Nitrogen Isotopic Analysis of Nitrate in Seawater and Freshwater *Anal. Chem.* **73** 4145–
1149 53

1150 Slavik K, Peterson B J, Deegan L A, Bowden W B, Hershey A E and Hobbie J E 2004 Long-Term Responses
1151 of the Kuparuk River Ecosystem to Phosphorus Fertilization *Ecology* **85** 939–54

1152 Strauss J, Schirrmeister L, Grosse G, Fortier D, Hugelius G, Knoblauch C, Romanovsky V, Schädel C,
1153 Schneider von Deimling T, Schuur E A G, Shmelev D, Ulrich M and Veremeeva A 2017 Deep
1154 Yedoma permafrost: A synthesis of depositional characteristics and carbon vulnerability *Earth-*
1155 *Science Reviews* **172** 75–86

1156 Striegl R G, Aiken G R, Dornblaser M M, Raymond P A and Wickland K P 2005 A decrease in discharge-
1157 normalized DOC export by the Yukon River during summer through autumn *Geophysical*
1158 *Research Letters* **32** Online: http://doi.wiley.com/10.1029/2005GL024413

1159 Sturm M, Racine C and Tape K 2001 Climate change: increasing shrub abundance in the Arctic *Nature*
1160 **411** 546–7

1161 Sturm M, Schimel J, Michaelson G, Welker J M, Oberbauer S F, Liston G E, Fahnestock J and Romanovsky
1162 V E 2005 Winter biological processes could help convert arctic tundra to shrubland *Bioscience* **55**
1163 17–26

1164 Tank S E, Striegl R G, McClelland J W and Kokelj S V 2016 Multi-decadal increases in dissolved organic
1165 carbon and alkalinity flux from the Mackenzie drainage basin to the Arctic Ocean *Environ. Res.*
1166 *Lett.* **11** 054015

1167 Tank S E, Vonk J E, Walvoord M A, McClelland J W, Laurion I and Abbott B W 2020 Landscape matters:
1168 Predicting the biogeochemical effects of permafrost thaw on aquatic networks with a state
1169 factor approach *Permafrost and Periglacial Processes* Online:
1170 https://onlinelibrary.wiley.com/doi/abs/10.1002/ppp.2057

1171 Temnerud J and Bishop K 2005 Spatial Variation of Streamwater Chemistry in Two Swedish Boreal
1172 Catchments:? Implications for Environmental Assessment *Environmental Science & Technology*
1173 **39** 1463–9

1174 Tierney J A, Hedin L O and Wurzburger N 2019 Nitrogen fixation does not balance fire-induced nitrogen
1175 losses in longleaf pine savannas *Ecology* **100** e02735

1176 Toohey R C, Herman-Mercer N M, Schuster P F, Mutter E A and Koch J C 2016 Multidecadal increases in
1177 the Yukon River Basin of chemical fluxes as indicators of changing flowpaths, groundwater, and
1178 permafrost *Geophysical Research Letters* **43** 12,120-12,130

1179 Toolik Environmental Data Center Team 2019 *Meterological monitoring program at Toolik, Alaska,*
1180 *Toolik Field Station* (Fairbanks, Alaska: Institute of Arctic Biology, University of Alaska Fairbanks)
1181 Online: https://toolik.alaska.edu/edc/

1182 Treat C C, Wollheim W M, Varner R K and Bowden W B 2016 Longer thaw seasons increase nitrogen
1183 availability for leaching during fall in tundra soils *Environ. Res. Lett.* **11** 064013

1184 Turetsky M R, Abbott B W, Jones M C, Anthony K W, Olefeldt D, Schuur E A G, Grosse G, Kuhry P,
1185 Hugelius G, Koven C, Lawrence D M, Gibson C, Sannel A B K and McGuire A D 2020 Carbon
1186 release through abrupt permafrost thaw *Nature Geoscience* **13** 138–43

1187 Turetsky M R, Abbott B W, Jones M C, Anthony K W, Olefeldt D, Schuur E A G, Koven C, McGuire A D,
1188 Grosse G, Kuhry P, Hugelius G, Lawrence D M, Gibson C and Sannel A B K 2019 Permafrost
1189 collapse is accelerating carbon release *Nature* **569** 32

1190 Vancoppenolle M, Bopp L, Madec G, Dunne J, Ilyina T, Halloran P R and Steiner N 2013 Future Arctic
1191 Ocean primary productivity from CMIP5 simulations: Uncertain outcome, but consistent
1192 mechanisms: FUTURE ARCTIC OCEAN PRIMARY PRODUCTIVITY *Global Biogeochemical Cycles* **27**
1193 605–19

1194 Viereck L A, Werdin-Pfisterer N R, Adams P C and Yoshikawa K 2008 Effect of wildfire and fireline
1195 construction on the annual depth of thaw in a black spruce permafrost forest in interior Alaska:
1196 a 36-year record of recovery *In: Kane, Douglas L.; Hinkel, Kenneth M., eds. Proceedings of the*
1197 *Ninth International Conference on Permafrost; June 29-July 3, 2008; Fairbanks, AK: 1845-1850.*
1198 Online: https://www.fs.usda.gov/treesearch/pubs/all/32468

1199 Vitousek P M and Reiners W A 1975 Ecosystem Succession and Nutrient Retention: A Hypothesis
1200 *BioScience* **25** 376–81

1201 Voigt C, Marushchak M E, Abbott B W, Biasi C, Elberling B, Siciliano S D, Sonnentag O, Stewart K J, Yang Y
1202 and Martikainen P J 2020 Nitrous oxide emissions from permafrost-affected soils *Nature*
1203 *Reviews Earth & Environment* 1–15

1204 Vonk J E, Tank S E, Bowden W B, Laurion I, Vincent W F, Alekseychik P, Amyot M, Billet M F, Canário J,
1205 Cory R M, Deshpande B N, Helbig M, Jammet M, Karlsson J, Larouche J, MacMillan G, Rautio M,
1206 Walter Anthony K M and Wickland K P 2015 Reviews and syntheses: Effects of permafrost thaw
1207 on Arctic aquatic ecosystems *Biogeosciences* **12** 7129–67

1208 Walker M D, Wahren C H, Hollister R D, Henry G H, Ahlquist L E, Alatalo J M, Bret-Harte M S, Calef M P,
1209 Callaghan T V, Carroll A B, and others 2006 Plant community responses to experimental
1210 warming across the tundra biome *Proceedings of the National Academy of Sciences of the*
1211 *United States of America* **103** 1342–6

1212 Walker X J, Baltzer J L, Cumming S G, Day N J, Ebert C, Goetz S, Johnstone J F, Potter S, Rogers B M,
1213 Schuur E A G, Turetsky M R and Mack M C 2019 Increasing wildfires threaten historic carbon sink
1214 of boreal forest soils *Nature* **572** 520–3

1215 Walvoord M A and Kurylyk B L 2016 Hydrologic Impacts of Thawing Permafrost—A Review *Vadose Zone*
1216 *Journal* **15** vzj2016.01.0010

1217 Wang J-J, Lafrenière M J, Lamoureux S F, Simpson A J, Gélinas Y and Simpson M J 2018 Differences in
1218 Riverine and Pond Water Dissolved Organic Matter Composition and Sources in Canadian High
1219 Arctic Watersheds Affected by Active Layer Detachments *Environ. Sci. Technol.* **52** 1062–71

1220 Wauthy M, Rautio M, Christoffersen K S, Forsström L, Laurion I, Mariash H L, Peura S and Vincent W F
1221 2018 Increasing dominance of terrigenous organic matter in circumpolar freshwaters due to
1222 permafrost thaw *Limnol. Oceanogr.* 1–13

1223 Wein R W and Bliss L C 1973 Changes in Arctic Eriophorum Tussock Communities Following Fire *Ecology*
1224 **54** 845–52

1225 Weishaar J L, Aiken G R, Bergamaschi B A, Fram M S, Fujii R and Mopper K 2003 Evaluation of specific
1226 ultraviolet absorbance as an indicator of the chemical composition and reactivity of dissolved
1227 organic carbon *Environmental Science & Technology* **37** 4702–8

1228 Weiss M, Hobbie S E and Gettel G M 2005 Contrasting Responses of Nitrogen-Fixation in Arctic Lichens
1229 to Experimental and Ambient Nitrogen and Phosphorus Availability *Arctic, Antarctic, and Alpine*
1230 *Research* **37** 396–401

1231 Wickham H, Chang W, Henry L, Pedersen T L, Takahashi K, Wilke C, Woo K, Yutani H, Dunnington D and
1232 RStudio 2020 ggplot2: Create Elegant Data Visualisations Using the Grammar of Graphics Online:
1233 https://CRAN.R-project.org/package=ggplot2

1234 Wickland K P, Neff J C and Aiken G R 2007 Dissolved Organic Carbon in Alaskan Boreal Forest: Sources,
1235 Chemical Characteristics, and Biodegradability *Ecosystems* **10** 1323–40

Wickland K P, Waldrop M P, Aiken G R, Koch J C, Jorgenson M T and Striegl R G 2018 Dissolved organic carbon and nitrogen release from boreal Holocene permafrost and seasonally frozen soils of Alaska *Environ. Res. Lett.* **13** 065011

Wieder W R, Cleveland C C, Smith W K and Todd-Brown K 2015 Future productivity and carbon storage limited by terrestrial nutrient availability *Nature Geoscience* **8** 441–4

Wieder W R, Lawrence D M, Fisher R A, Bonan G B, Cheng S J, Goodale C L, Grandy A S, Koven C D, Lombardozzi D L, Oleson K W and Thomas R Q 2019 Beyond Static Benchmarking: Using Experimental Manipulations to Evaluate Land Model Assumptions *Global Biogeochemical Cycles* **33** 1289–309

Wild B, Andersson A, Bröder L, Vonk J, Hugelius G, McClelland J W, Song W, Raymond P A and Gustafsson Ö 2019 Rivers across the Siberian Arctic unearth the patterns of carbon release from thawing permafrost *PNAS* **116** 10280–5

Wologo E, Shakil S, Zolkos S, Textor S, Ewing S, Klassen J, Spencer R G M, Podgorski D C, Tank S E, Baker M A, O'Donnell J A, Wickland K P, Foks S S W, Zarnetske J P, Lee-Cullin J, Liu F, Yang Y, Kortelainen P, Kolehmainen J, Dean J F, Vonk J E, Holmes R M, Pinay G, Powell M M, Howe J, Frei R J, Bratsman S P and Abbott B W 2020 Stream dissolved organic matter in permafrost regions shows surprising compositional similarities but negative priming and nutrient effects *Global Biogeochemical Cycles* e2020GB006719

Wright K S and Rocha A V 2018 A test of functional convergence in carbon fluxes from coupled C and N cycles in Arctic tundra *Ecological Modelling* **383** 31–40

Wymore A S, Leon M C, Shanley J B and McDowell W H 2019 Hysteretic Response of Solutes and Turbidity at the Event Scale Across Forested Tropical Montane Watersheds *Front. Earth Sci.* **7** Online: https://www.frontiersin.org/articles/10.3389/feart.2019.00126/full

Yoshikawa K, Bolton W R, Romanovsky V E, Fukuda M and Hinzman L D 2002 Impacts of wildfire on the permafrost in the boreal forests of Interior Alaska *Journal of Geophysical Research: Atmospheres* **107** FFR 4-1-FFR 4-14

Zamin T J and Grogan P 2012 Birch shrub growth in the low Arctic: the relative importance of experimental warming, enhanced nutrient availability, snow depth and caribou exclusion *Environmental Research Letters* **7** 034027

Zarnetske J P, Bouda M, Abbott B W, Saiers J and Raymond P A 2018 Generality of Hydrologic Transport Limitation of Watershed Organic Carbon Flux Across Ecoregions of the United States *Geophysical Research Letters* **45** 11,702-11,711

Zimov N S, Zimov S A, Zimova A E, Zimova G M, Chuprynin V I and Chapin F S 2009 Carbon storage in permafrost and soils of the mammoth tundra-steppe biome: Role in the global carbon budget: CARBON STORAGE OF THE MAMMOTH STEPPE *Geophysical Research Letters* **36** Online: http://doi.wiley.com/10.1029/2008GL036332

1272 Zolkos S and Tank S E 2020 Experimental Evidence That Permafrost Thaw History and Mineral
1273 Composition Shape Abiotic Carbon Cycling in Thermokarst-Affected Stream Networks *Front.*
1274 *Earth Sci.* **8** 152

1275

1276

Tables and figures

Table 1. Dates and conditions for the six samplings

Date	Daily Q ($L\ m^{-2}\ day^{-1}$)	Weekly Q ($L\ m^{-2}\ day^{-1}$)	Monthly precip. (mm)	Daily air temp. (°C)**	Weekly air temp. (°C)	Monthly air temp. (°C)	Thaw depth, unburned (cm)	Thaw depth, burned (cm)	n burned	n unburned
9-Jun-17	5.09*	6.03*	5.0	1.75	2.57	8.03	9.5	11.9	21	15
30-Jul-17	3.51	2.30	108	10.5	13.3	12.6	37.5	44.1	21	21
31-Aug-17	1.44	2.02	103	-3.04	-1.03	5.65	53.1	63.6	8	11
5-Jun-18	22.2*	18.7*	38	4.76	4.06	4.85	7.0***	12.6***	21	21
20-Jul-18	4.50	4.05	115	6.63	9.50	10.3	34.4	40.8	21	21
25-Aug-18	1.33	1.51	129	3.41	4.05	4.21	49.7	56.3	21	21

*Data for these dates was inferred based on lower Kuparuk station, **All air temperature data from a 3m height at the Toolik Field Station, ***Thaw depths for this date were interpolated because there was more than a week difference between thaw depth measurements and aquatic sampling

Table 2. Lateral flux (±SE) of organic nutrients from unburned and burned watersheds

Year	Q ($L\ m^{-2}\ yr^{-1}$)	State	DOC ($mg\ m^{-2}\ yr^{-1}$)	DON ($mg\ m^{-2}\ yr^{-1}$)	DOP ($mg\ m^{-2}\ yr^{-1}$)	DOS ($mg\ m^{-2}\ yr^{-1}$)
2017	319	Unburned	3,660 ±190	151 ±4.6	1.58 ±0.21	39.1 ±3.4
		Burned	4,640 ±273	211 ±8.5	2.27 ±0.43	54.1 ±4.7
		Δ (%)	27.0	40.4	44.3	38.2
2018	702	Unburned	7,310 ±287	210 ±16.7	5.19 ±0.61	37.5 ±4.6
		Burned	9,050 ±266	360 ±17.8	8.90 ±0.73	58.9 ±13.5
		Δ (%)	23.8	71.7	71.6	56.9
Interannual mean		Unburned	5,480 ±256	180 ±10.7	3.38 ±0.41	38.3 ±4.0
		Burned	6,850 ±268	286 ±13.1	5.59 ±0.58	56.5 ±9.1
		Δ (%)	24.9	58.6	65.2	47.4

1283

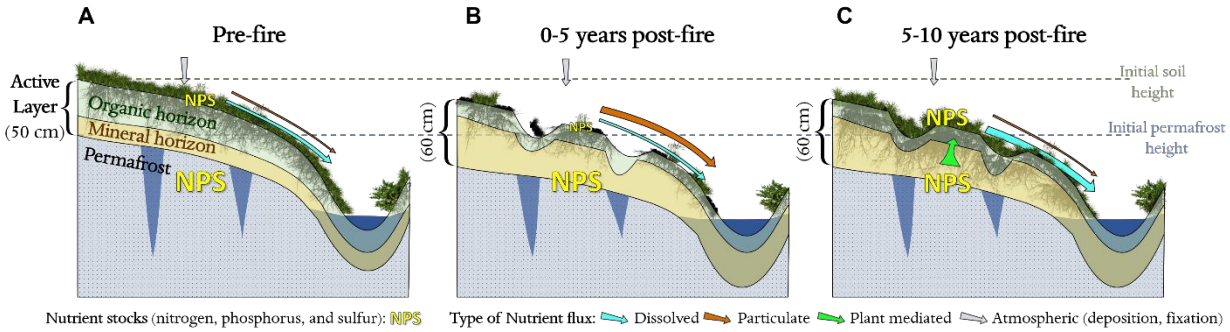

1284

1285 **Figure 1.** Conceptual diagram of wildfire effects on nutrient balance in Arctic tundra. (A) Pre-disturbance, there is
1286 low nutrient availability in the active layer because of limited decomposition and high demand from microorganisms
1287 and plants. There are large stores of nitrogen (N), phosphorus (P), and sulfur (S) in permafrost. (B) Combustion,
1288 thermo-erosion, and high demand from regrowth exacerbate nutrient limitation on land while increasing erosion and
1289 associated flux of particulate nutrients. (C) Regrowth stabilizes erosion while plants take up deeper nutrients,
1290 enhancing lateral flux of dissolved organic nutrients.

1291

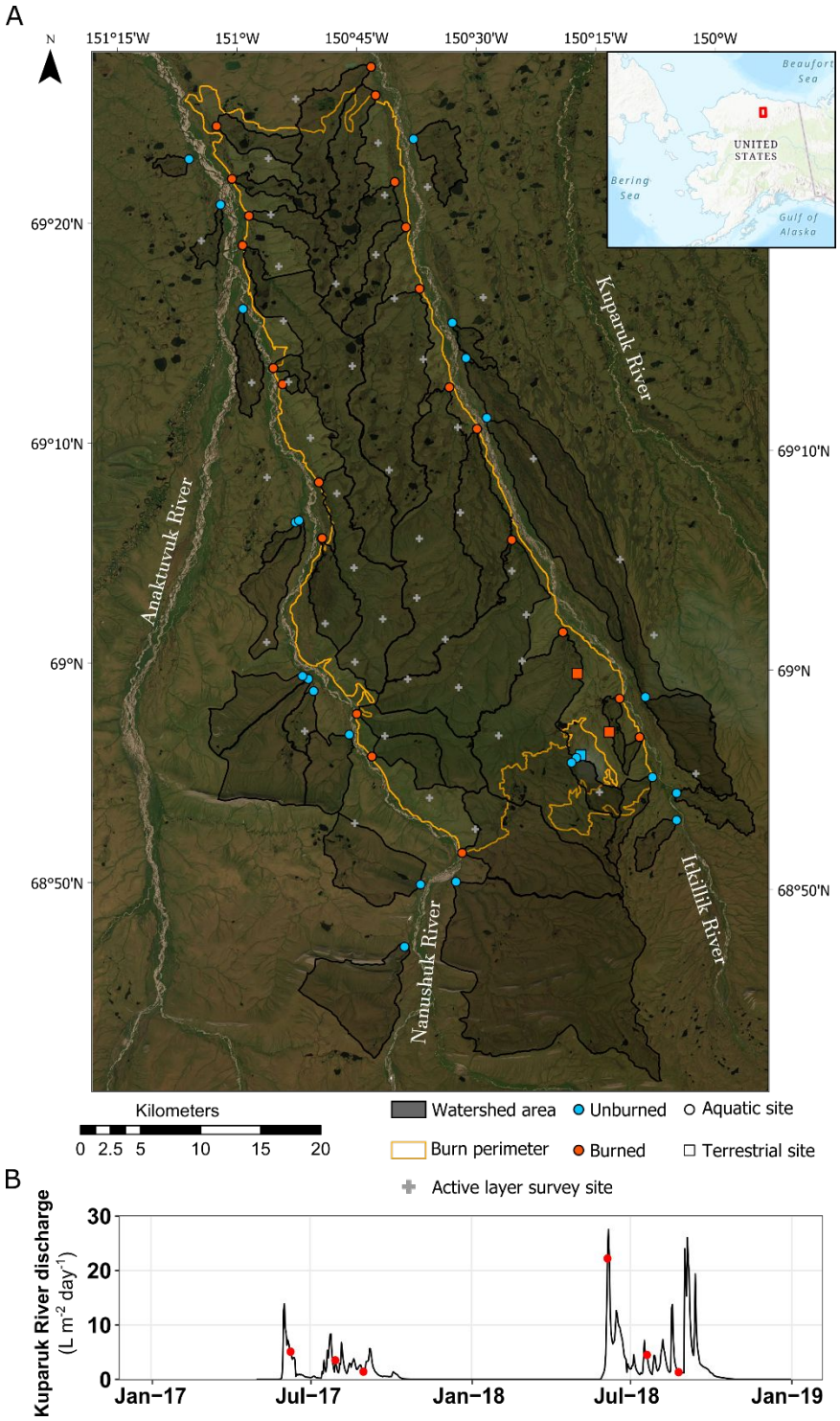

Figure 2. Map of the watersheds in and around the 2007 Anaktuvuk River wildfire **(A)**, and hydrograph of the Kuparuk River **(B)**. Stream samples were collected 6 times at the 42 watershed outlets (colored circles). Active-layer depth and plant and soil C and N content were measured at the 3 terrestrial sites (colored squares). Active layer thickness was measured at 47 additional sites (gray crosses) in 2014 and 2019. Panel B shows specific discharge for the closest river with continuous flow data, with the sampling dates indicated by the red dots.

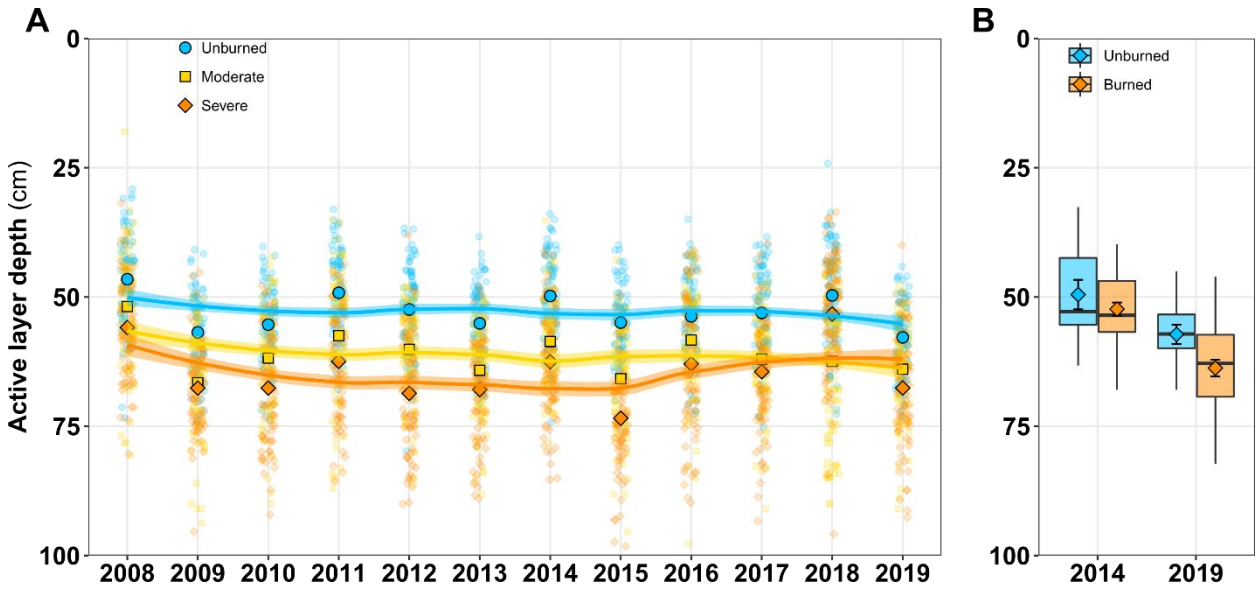

Figure 3. Active layer thickness (maximum seasonal depth of thaw) based on thaw-probe measurements. **(A)** Observations from the three terrestrial sites where active layer was measured yearly in late August or early September from 2008 to 2019. The outlined shapes represent the mean for that site and date, and the fitted lines show the smoothed conditional means and standard error across the period of observation. **(B)** Results of the active layer surveys done in 2014 and 2019 at 47 sites distributed within and near the burn scar (Fig. 2). Box plots represent median, quartiles, 1.5 times the interquartile range (IQR), and points beyond 1.5 times the IQR. The diamonds and error bars represent the mean and standard error.

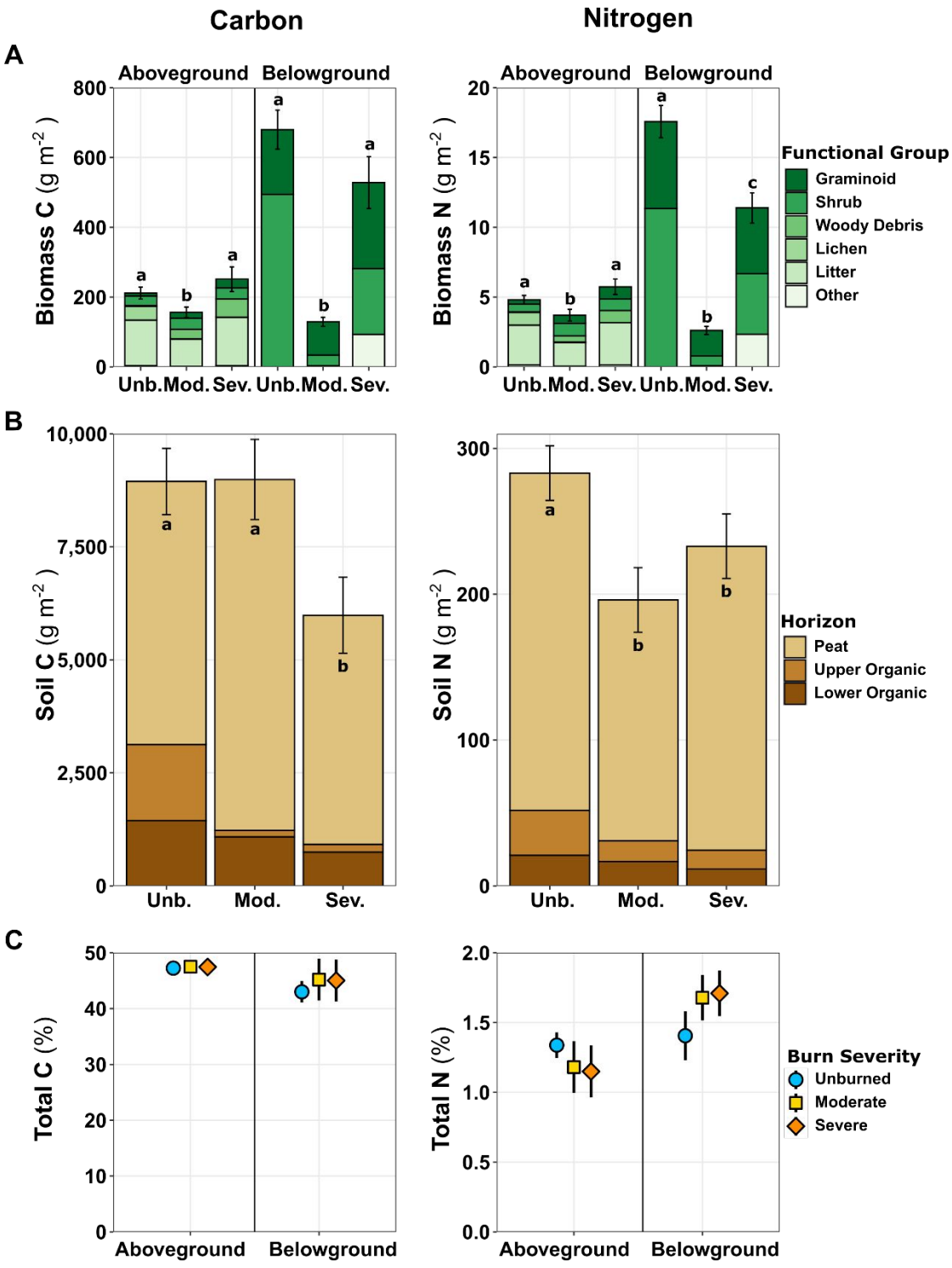

Figure 4. Plant biomass C and N content in biomass **(A)**, peat and organic soil **(B)**, and overall percent C and N **(C)**. Bars and points represent the among-location mean and standard error, with letters indicating statistically significant differences. Data were collected in 2017 from the unburned, moderately burned, and severely burned sites in or near the fire scar (Fig. 2).

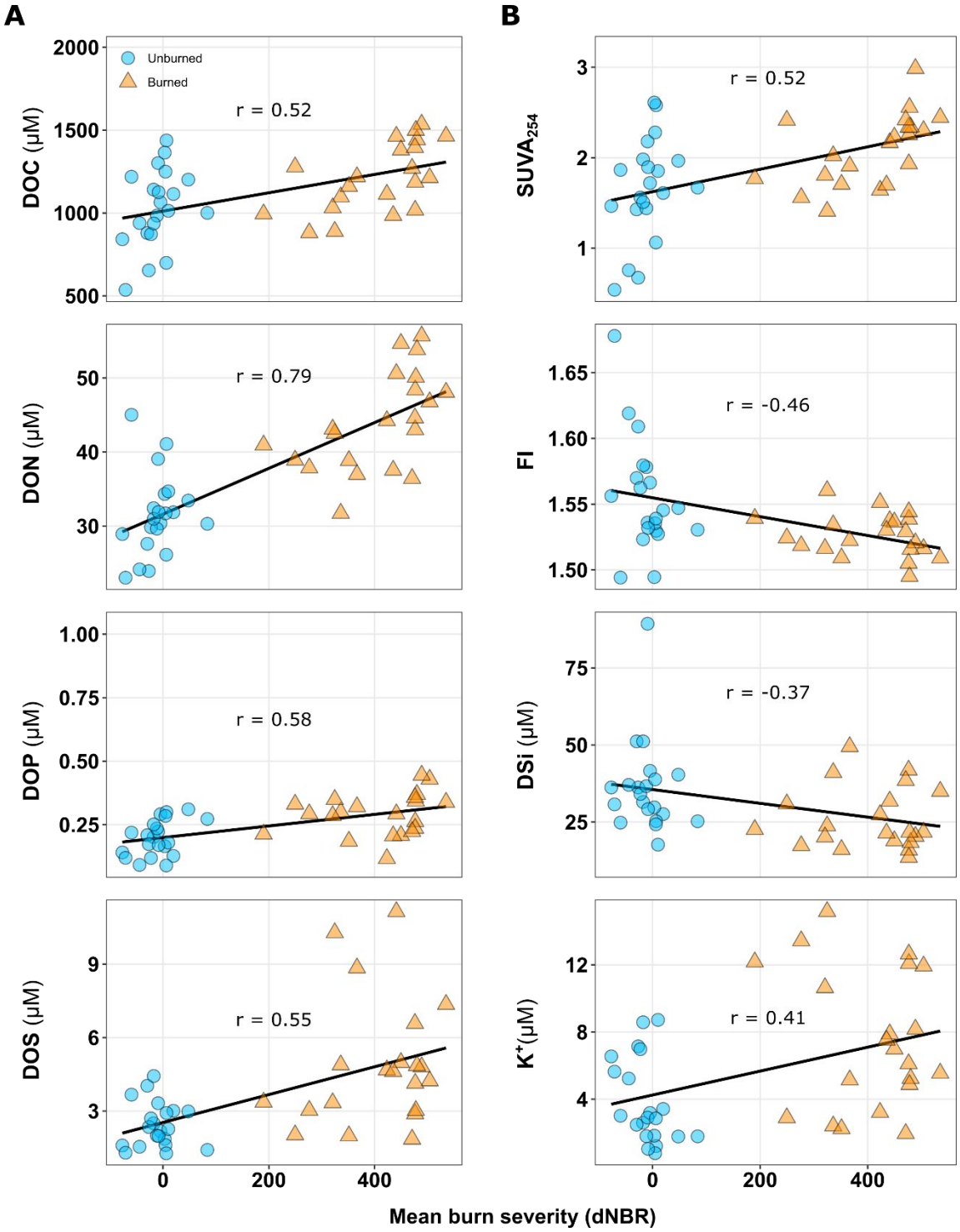

Figure 5. Significant Pearson correlations ($p < 0.05$) between burn severity and mean concentrations of **(A)** organic nutrients, and **(B)** optical properties, dissolved silica, and potassium for 21 burned and 21 unburned watersheds. For correlation coefficients and p-values for all chemical parameters, see Fig. 6 and Tables S3 and S4.

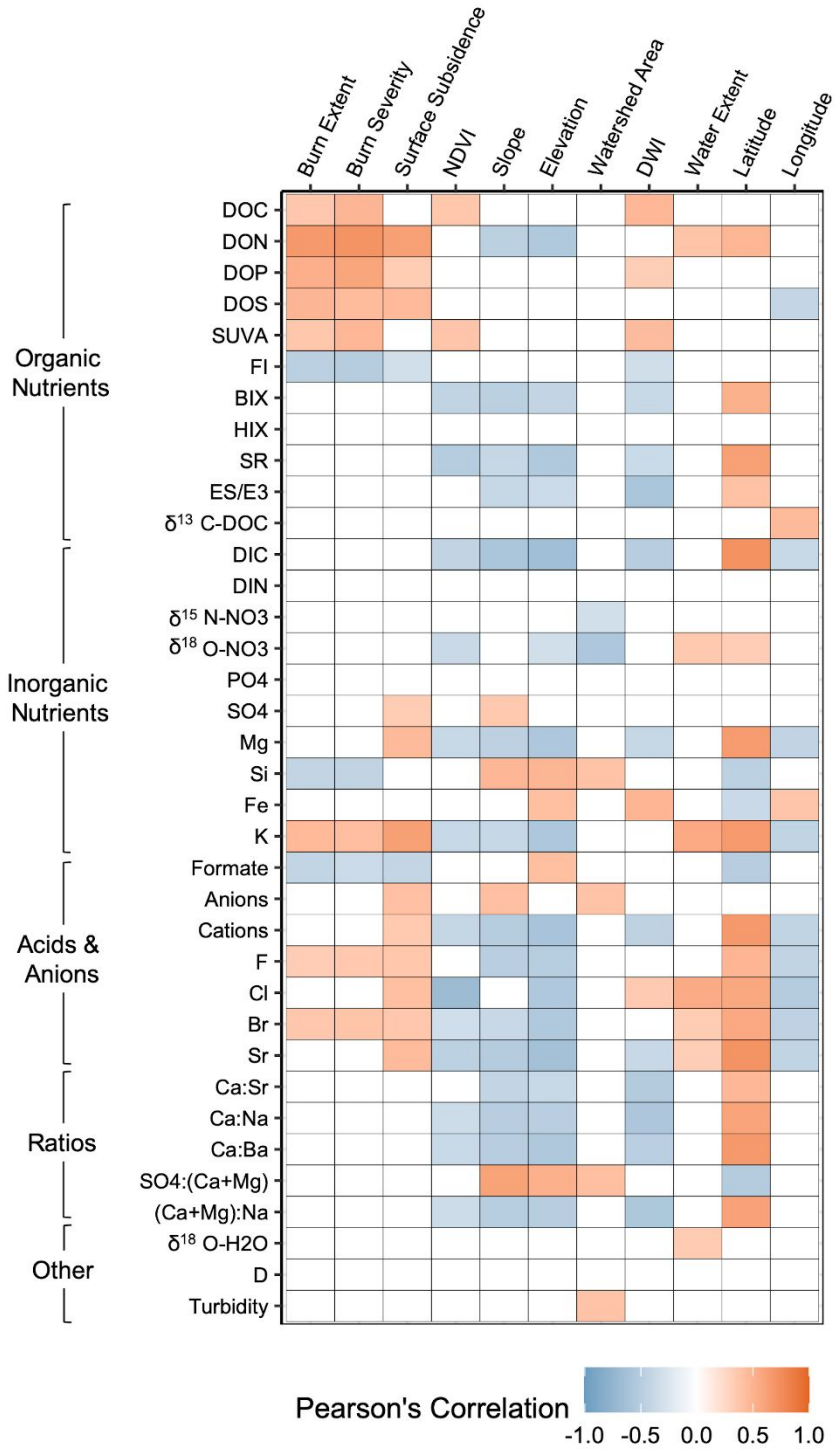

1315

1316 **Figure 6.** Correlation coefficients among catchment characteristics and mean water chemistry parameters. Only
1317 significant correlations ($p < 0.05$) are shown. For correlation coefficients and p-values for all parameters, see Tables
1318 S3 and S4.

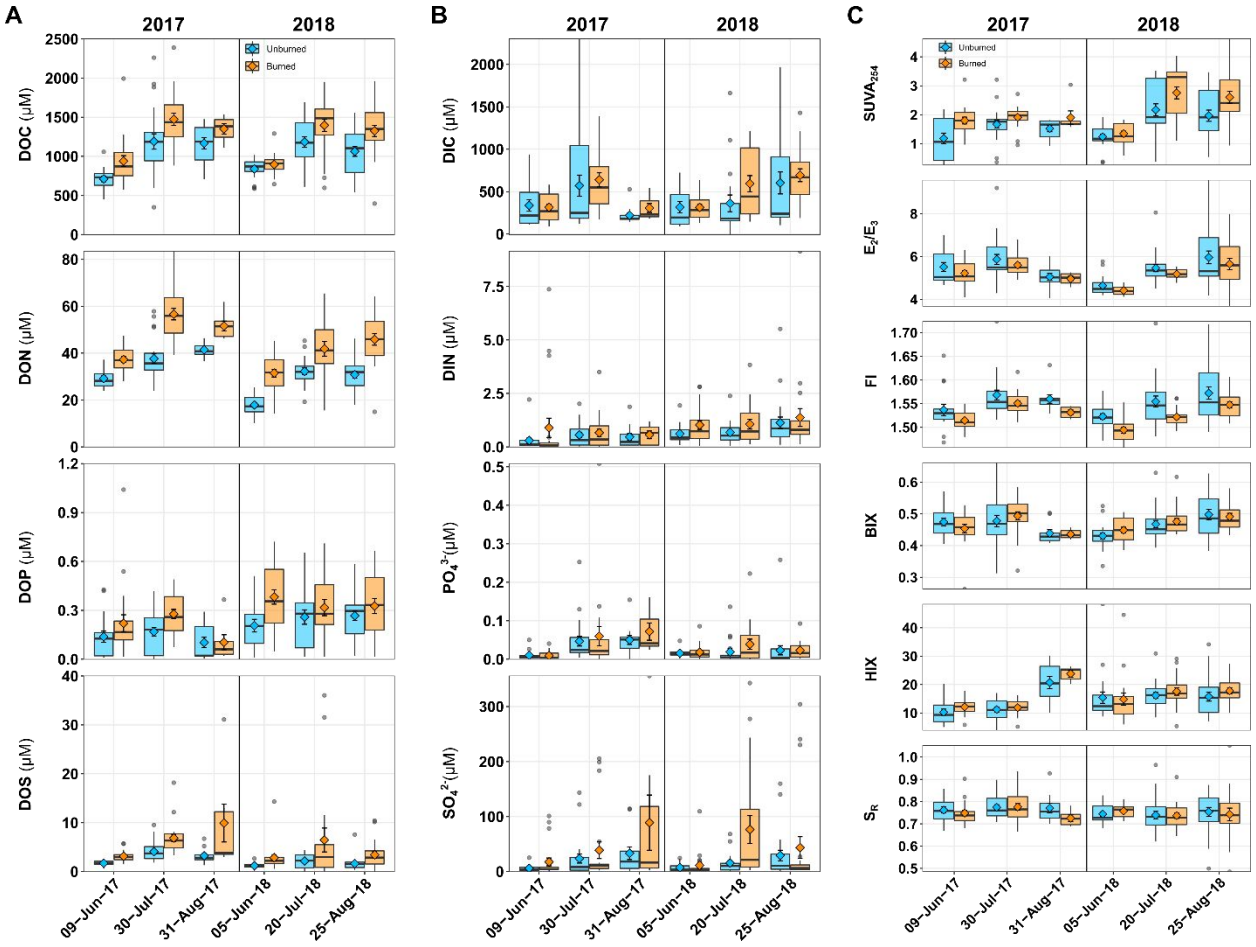

Figure 7. Seasonal concentrations of organic nutrients **(A)**, inorganic nutrients **(B)**, and optical properties of dissolved organic matter **(C)**, in streams draining the burned (n=21) and unburned (n=21) watersheds. Symbology follows Figure 3B. For detailed interpretation of optical properties, see Table S1.

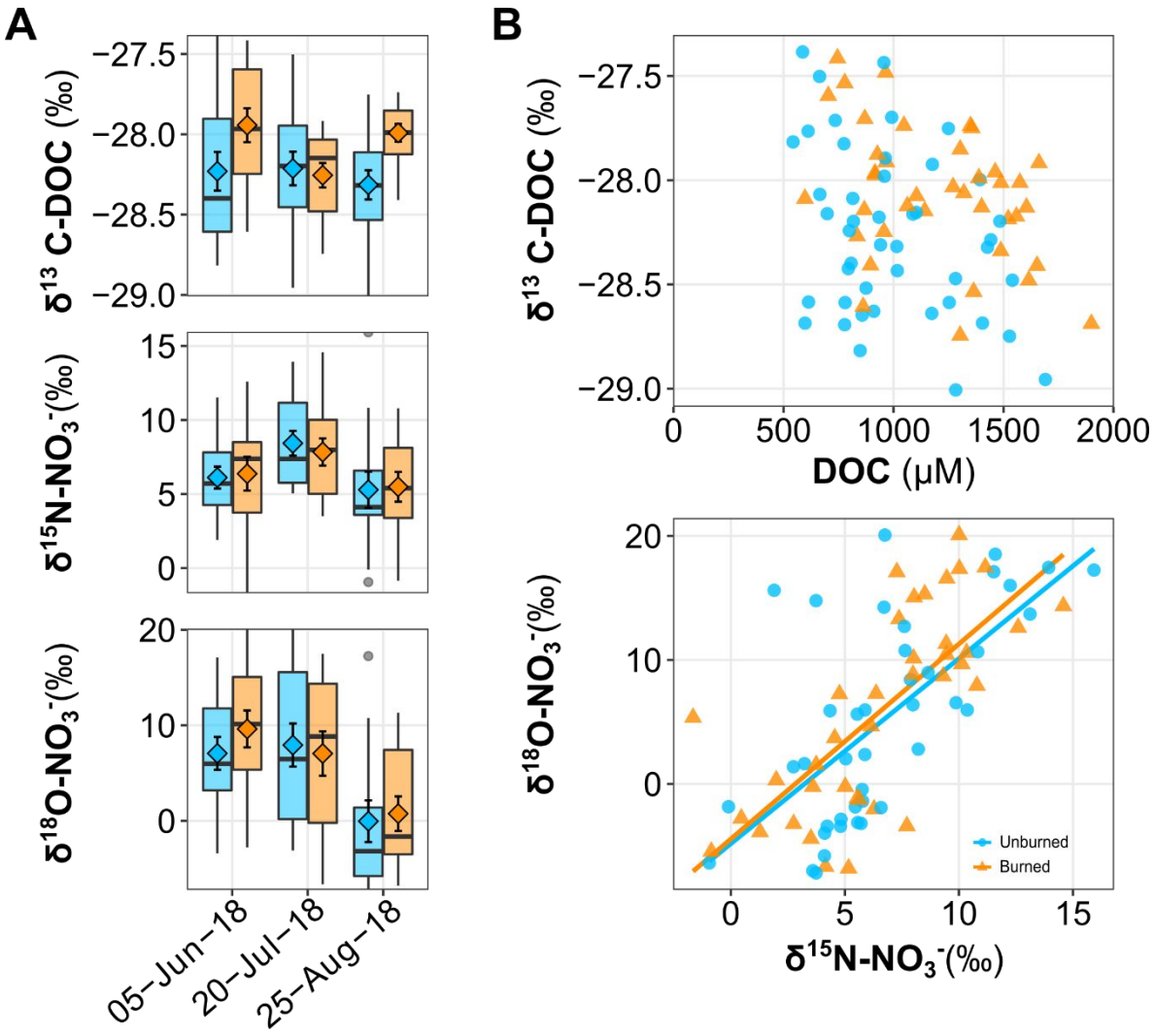

Figure 8. Stable isotopes of DOC and NO_3^-. **(A)** Seasonal changes in isotopic values for burned and unburned watersheds. Symbology follows Figure 3B. **(B)** Relationships of DOC concentration with $\delta^{13}C$ and NO_3^- isotopes.

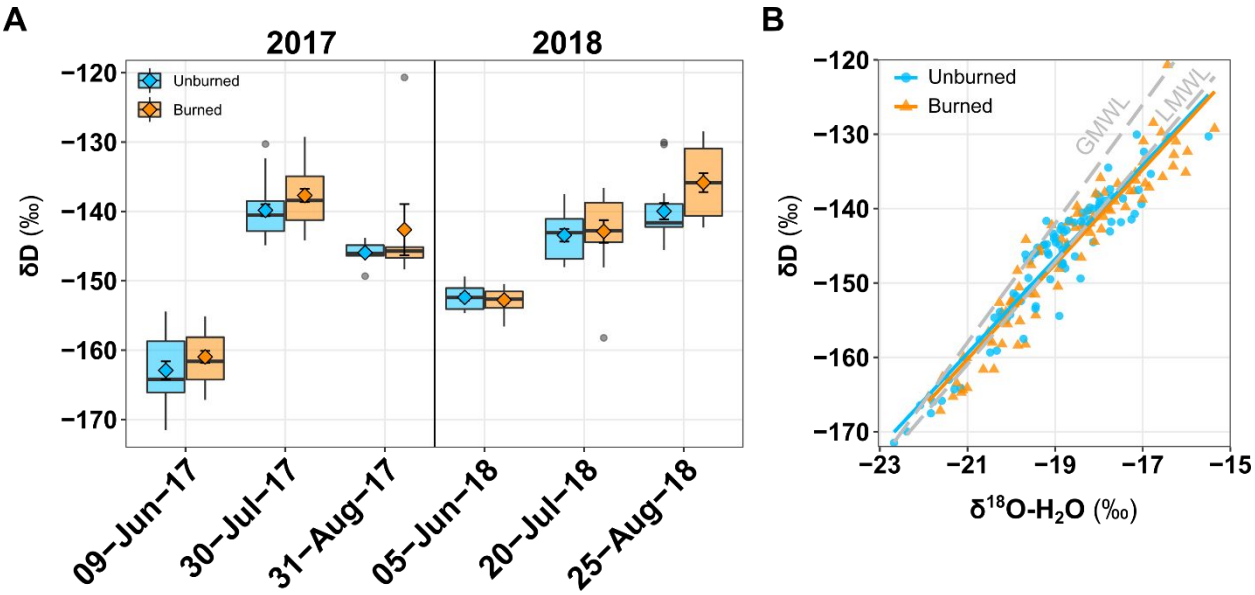

1326

1327 **Figure 9**. Seasonal variation in water isotopes **(A)** and the local evaporation lines between $\delta^{18}O$ and δD
1328 **(B)** in stream water. The global and local meteoric water lines are shown for reference (GMWL and
1329 LMWL, respectively). LMWL was calculated with precipitation measurements from the nearby Kuparuk
1330 River watershed (Harms and Godsey 2017). Boxplot symbology follows Figure 3B.

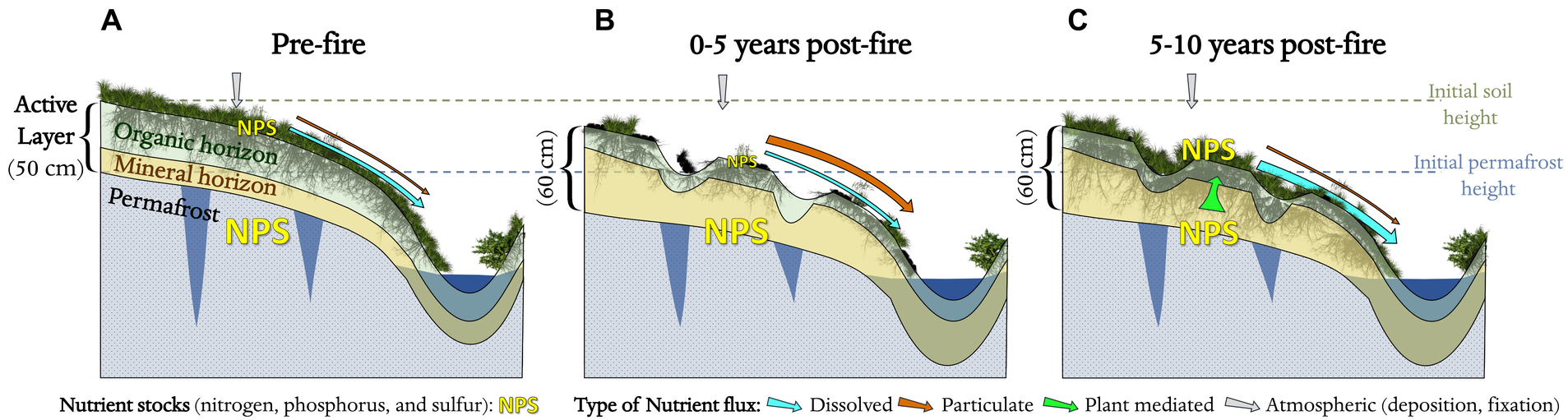
A
Pre-fire
B
0-5 years post-fire
C
5-10 years post-fire
Active Layer (50 cm)
Organic horizon
Mineral horizon
Permafrost
NPS
(60 cm)
Initial soil height
Initial permafrost height
Nutrient stocks (nitrogen, phosphorus, and sulfur): NPS
Type of Nutrient flux: Dissolved Particulate Plant mediated Atmospheric (deposition, fixation)

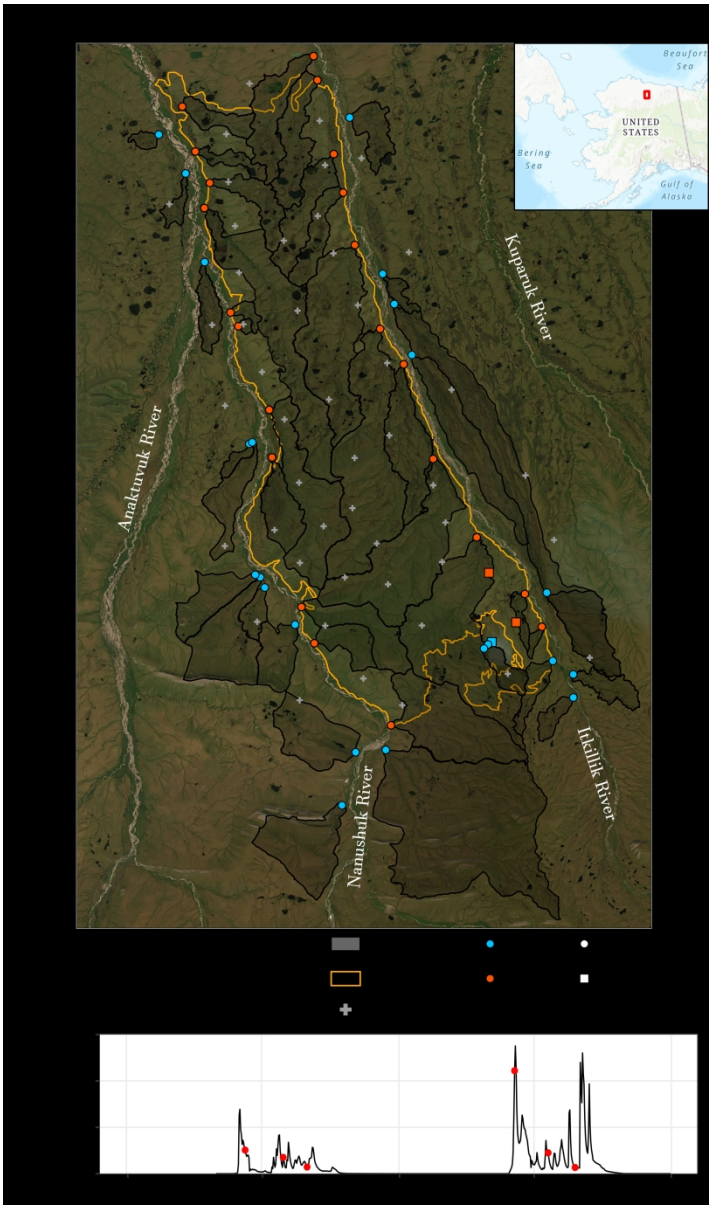

Figure 2. Map of the watersheds in and around the 2007 Anaktuvuk River wildfire (A), and hydrograph of the Kuparuk River (B). Stream samples were collected 6 times at the 42 watershed outlets (colored circles). Active-layer depth and plant and soil C and N content were measured at the 3 terrestrial sites (colored squares). Active layer thickness was measured at 47 additional sites (gray crosses) in 2014 and 2019. Panel B shows specific discharge for the closest river with continuous flow data, with the sampling dates indicated by the red dots.

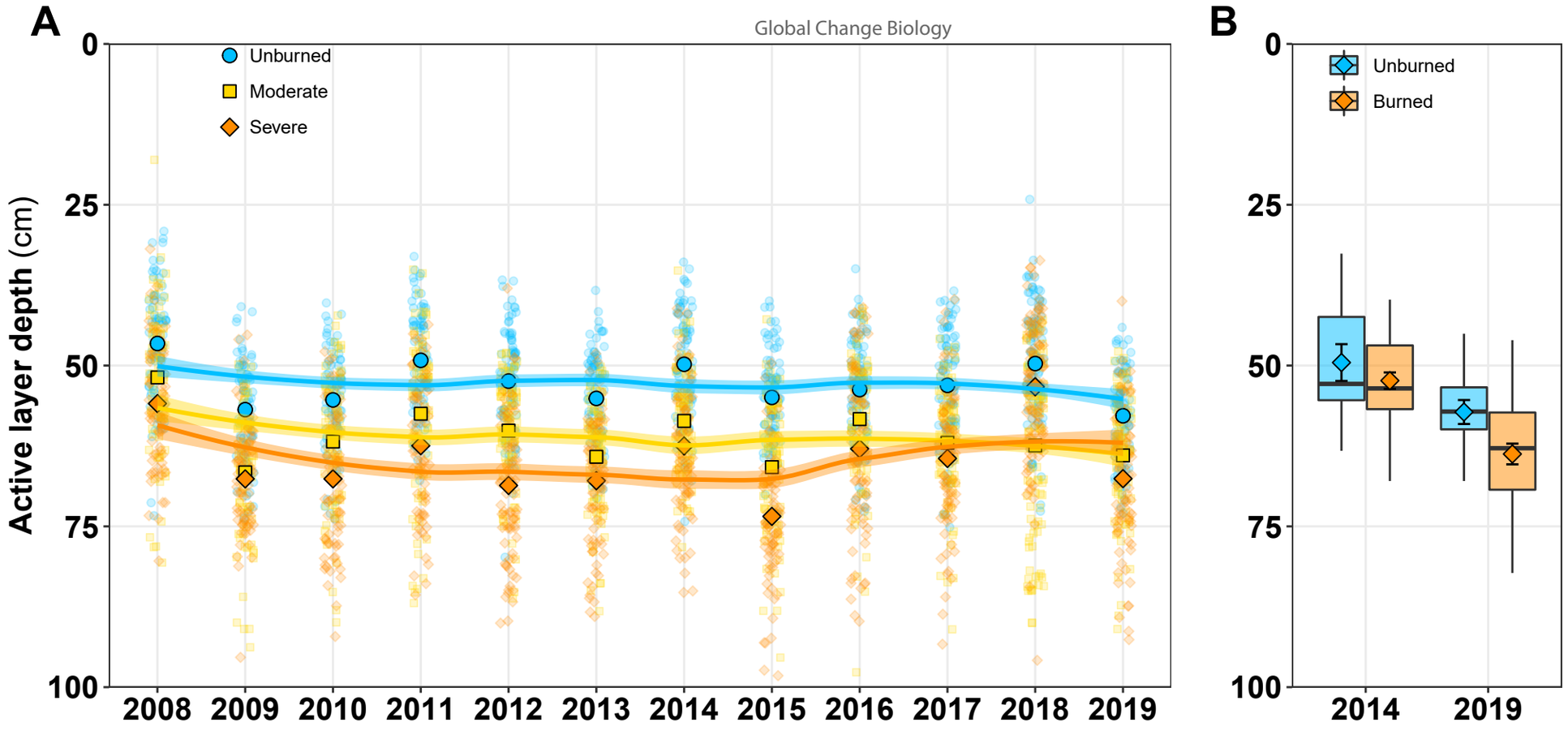
A
B
Unburned
Moderate
Severe
Burned
Active layer depth (cm)
0
25
50
75
100
2008
2009
2010
2011
2012
2013
2014
2015
2016
2017
2018
2019

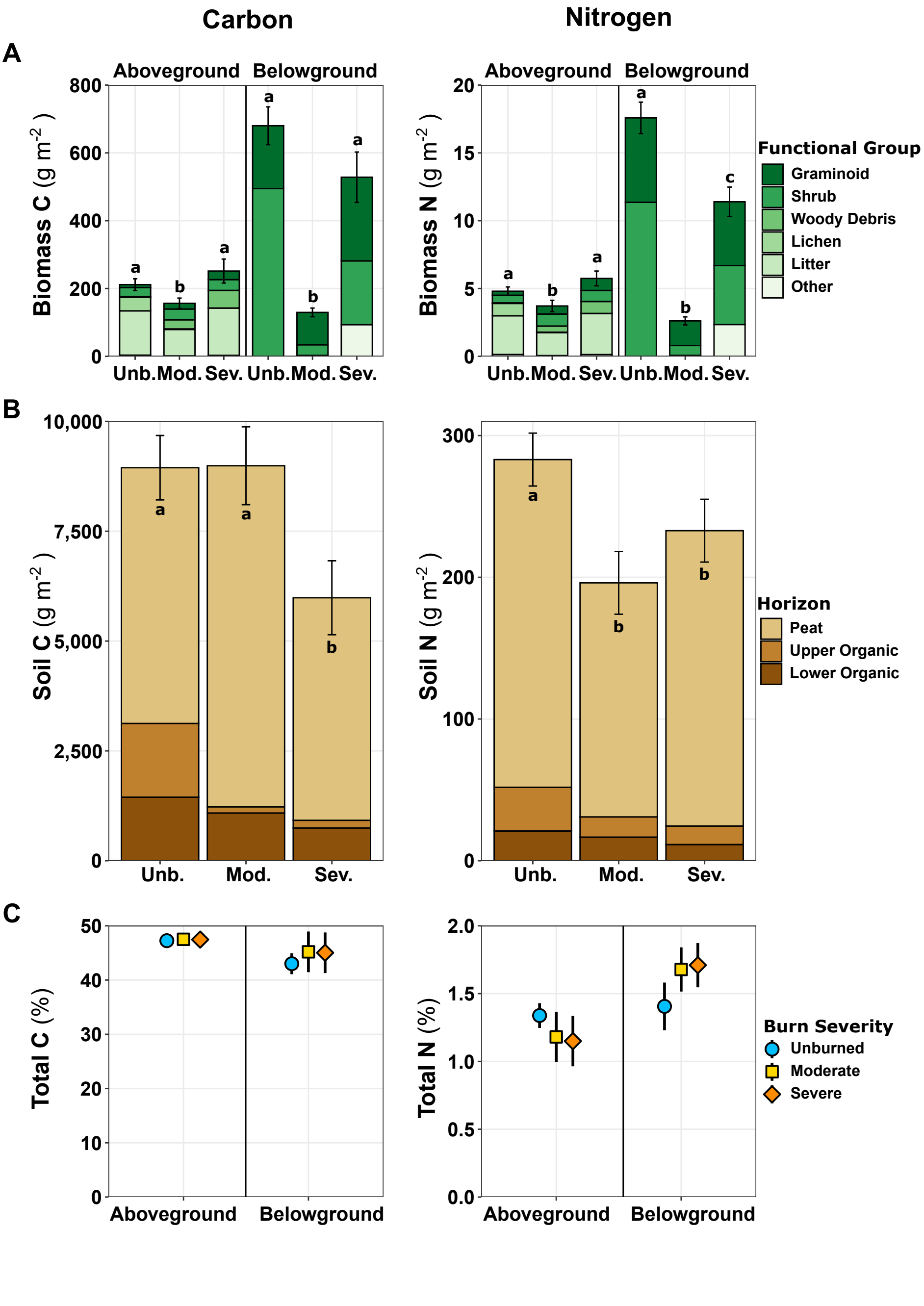
Carbon
Nitrogen
A
Aboveground
Belowground
Biomass C (g m-2)
Biomass N (g m-2)
Unb.
Mod.
Sev.
Functional Group
Graminoid
Shrub
Woody Debris
Lichen
Litter
Other
B
Soil C (g m-2)
Soil N (g m-2)
Horizon
Peat
Upper Organic
Lower Organic
C
Total C (%)
Total N (%)
Burn Severity
Unburned
Moderate
Severe

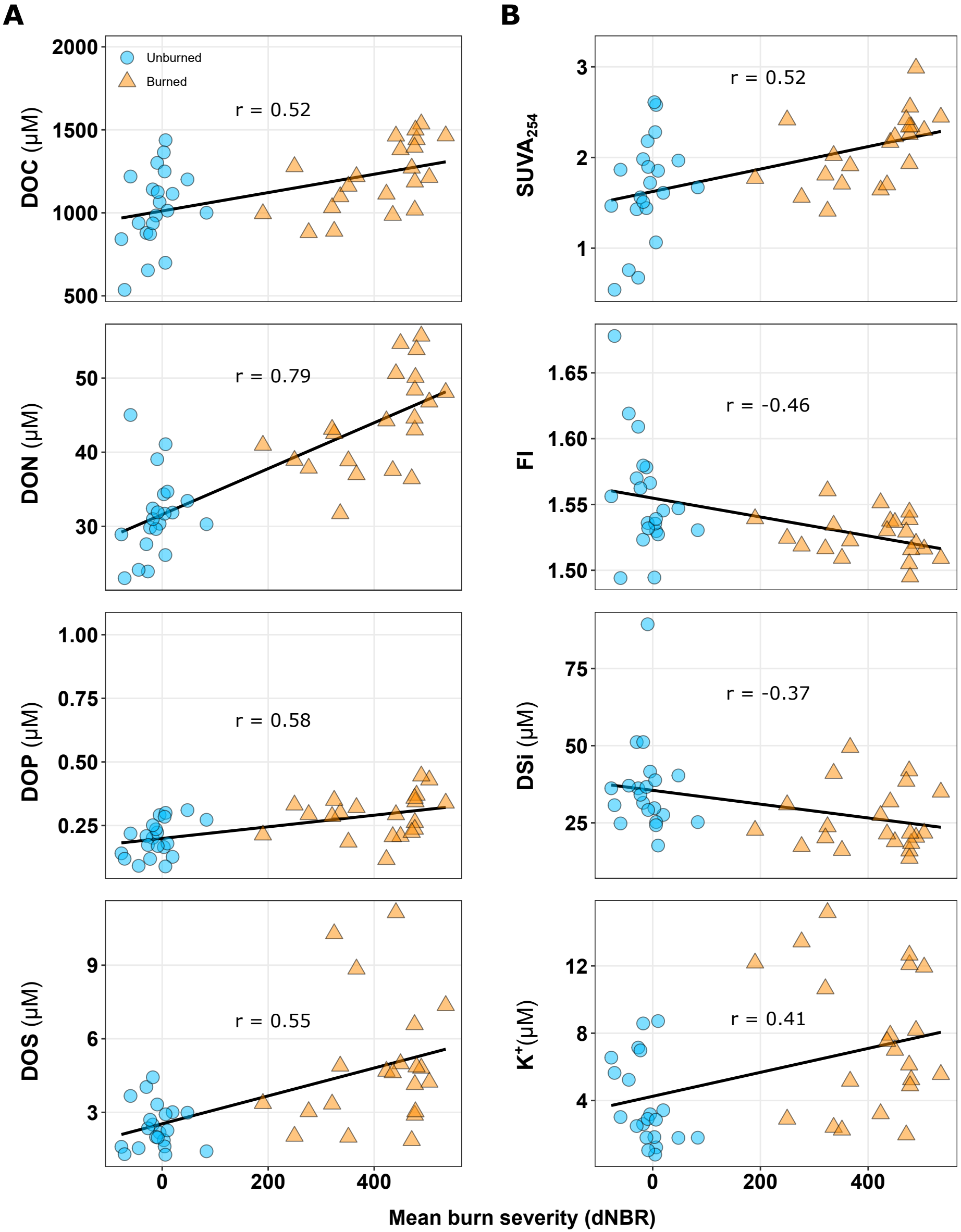
A
B
Unburned
Burned
DOC (µM)
r = 0.52
SUVA254
r = 0.52
DON (µM)
r = 0.79
FI
r = -0.46
DOP (µM)
r = 0.58
DSi (µM)
r = -0.37
DOS (µM)
r = 0.55
K+(µM)
r = 0.41
Mean burn severity (dNBR)

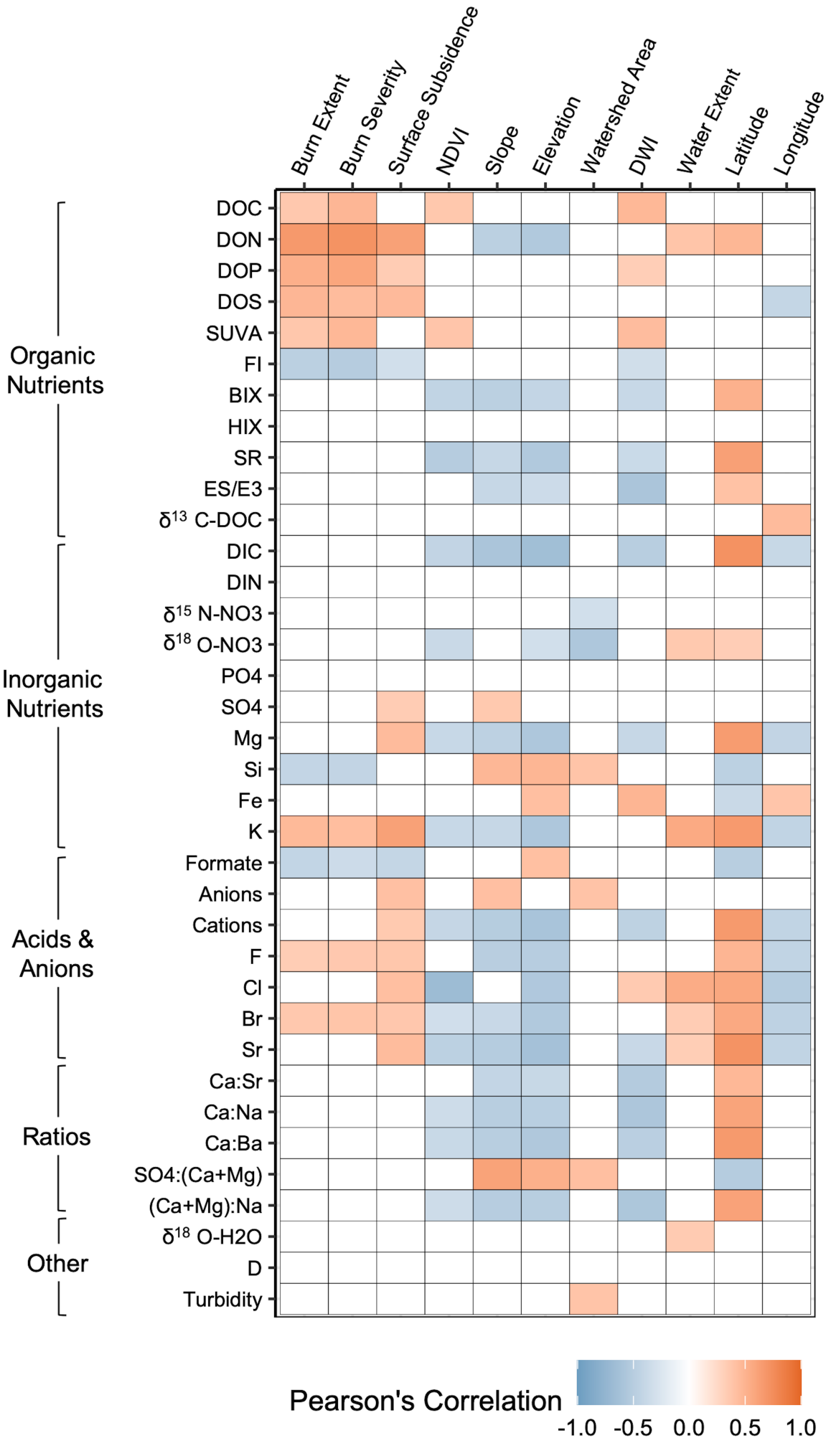
Burn Extent
Burn Severity
Surface Subsidence
NDVI
Slope
Elevation
Watershed Area
DWI
Water Extent
Latitude
Longitude
DOC
DON
DOP
DOS
SUVA
FI
BIX
HIX
SR
ES/E3
δ13 C-DOC
DIC
DIN
δ15 N-NO3
δ18 O-NO3
PO4
SO4
Mg
Si
Fe
K
Formate
Anions
Cations
F
Cl
Br
Sr
Ca:Sr
Ca:Na
Ca:Ba
SO4:(Ca+Mg)
(Ca+Mg):Na
δ18 O-H2O
D
Turbidity
Organic Nutrients
Inorganic Nutrients
Acids & Anions
Ratios
Other
Pearson's Correlation
-1.0 -0.5 0.0 0.5 1.0

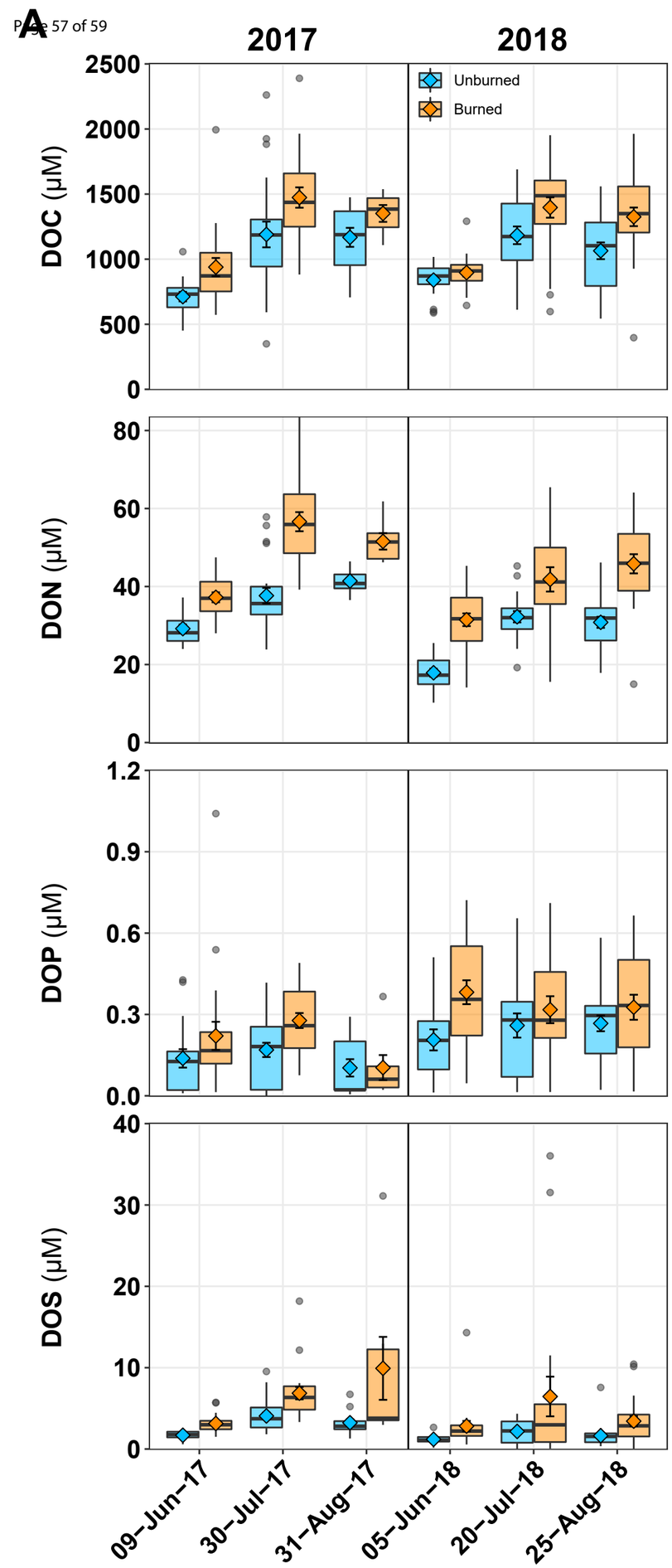
A
2017
2018
Unburned
Burned
DOC (μM)
DON (μM)
DOP (μM)
DOS (μM)
09–Jun–17
30–Jul–17
31–Aug–17
05–Jun–18
20–Jul–18
25–Aug–18

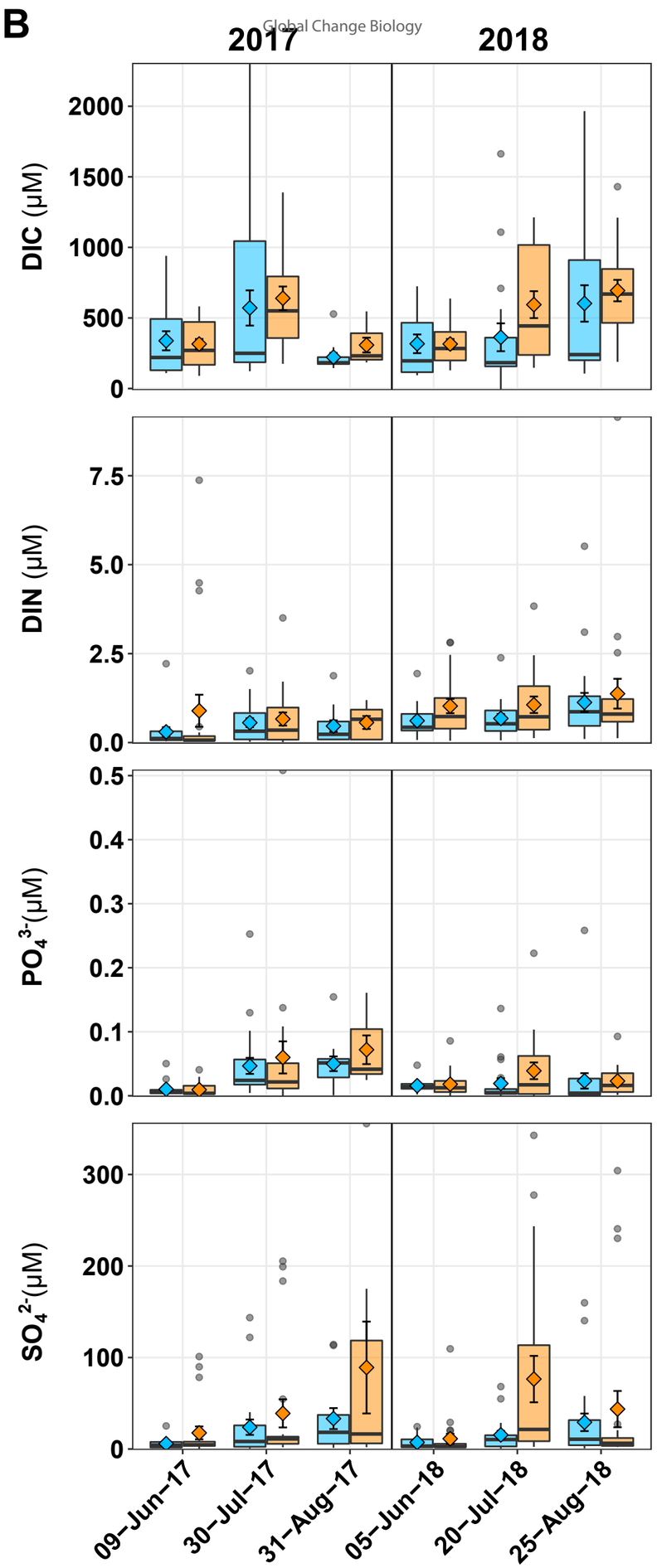
B
2017
2018
DIC (μM)
DIN (μM)
PO_4^{3-}(μM)
SO_4^{2-}(μM)
09–Jun–17
30–Jul–17
31–Aug–17
05–Jun–18
20–Jul–18
25–Aug–18

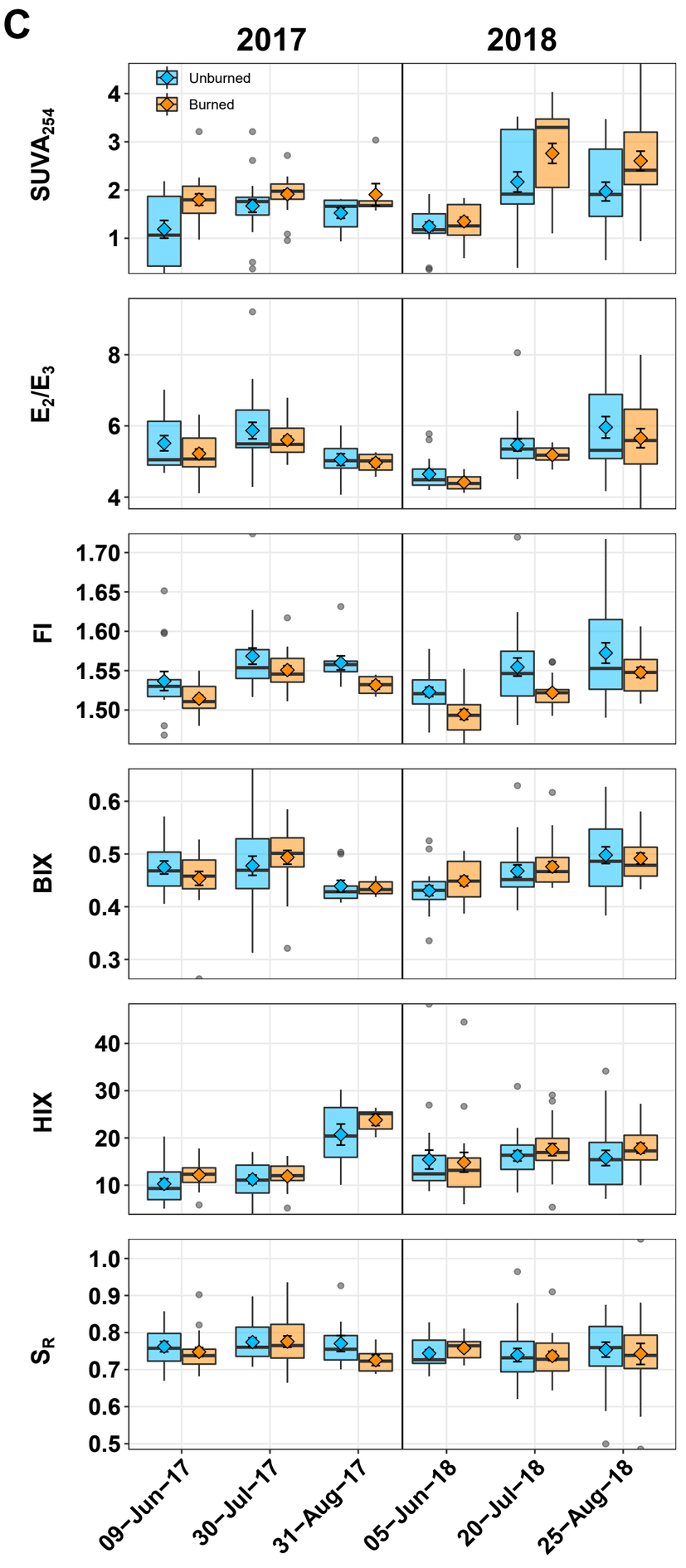
C
2017
2018
Unburned
Burned
$SUVA_{254}$
E_2/E_3
FI
BIX
HIX
S_R
09–Jun–17
30–Jul–17
31–Aug–17
05–Jun–18
20–Jul–18
25–Aug–18

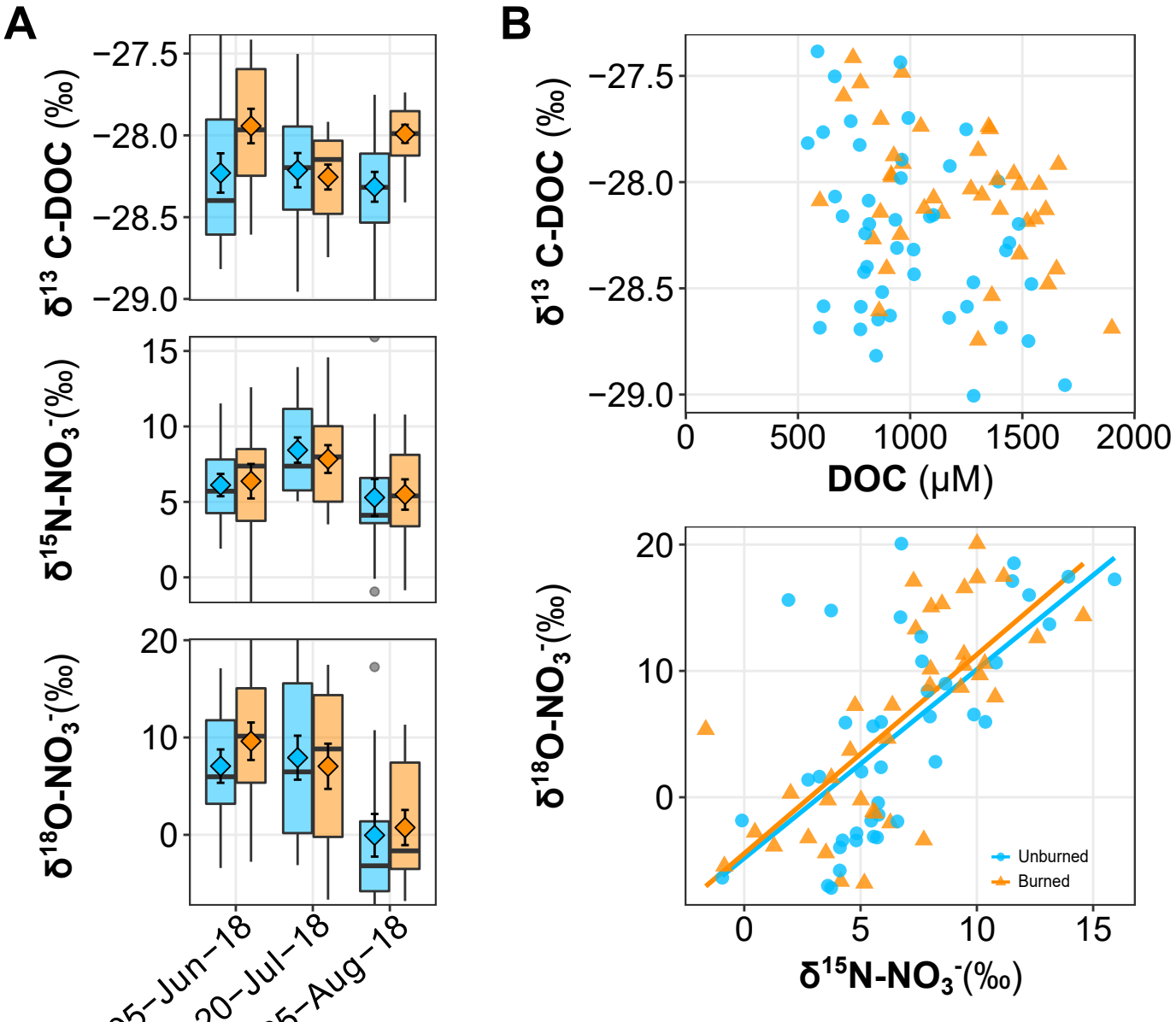
A
B
δ13 C-DOC (‰)
−27.5
−28.0
−28.5
−29.0
δ15N-NO3-(‰)
15
10
5
0
δ18O-NO3-(‰)
20
10
0
05−Jun−18
20−Jul−18
25−Aug−18
DOC (μM)
0
500
1000
1500
2000
δ15N-NO3-(‰)
0
5
10
15
Unburned
Burned

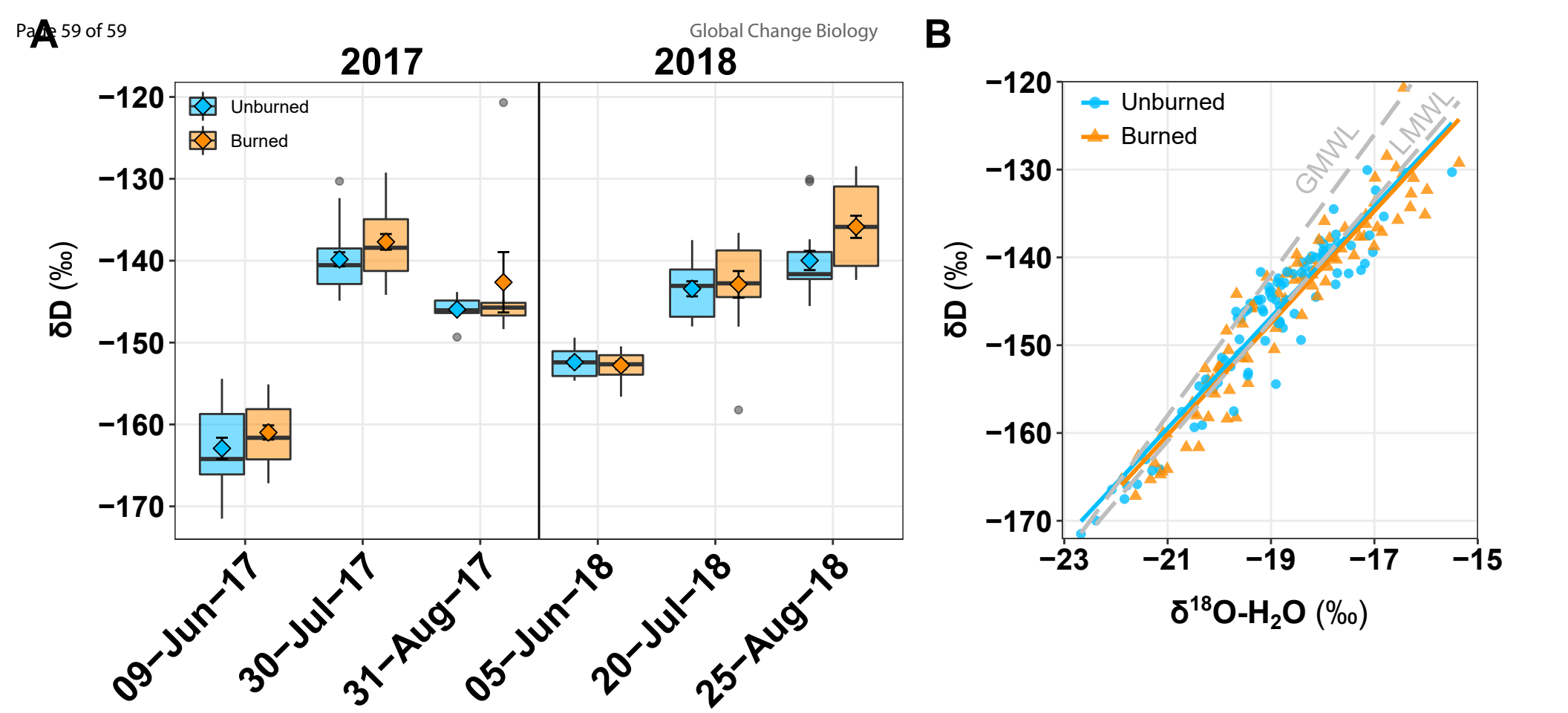
A
2017
2018
Unburned
Burned
δD (‰)
−120
−130
−140
−150
−160
−170
09−Jun−17
30−Jul−17
31−Aug−17
05−Jun−18
20−Jul−18
25−Aug−18
B
Unburned
Burned
GMWL
LMWL
δD (‰)
−120
−130
−140
−150
−160
−170
−23
−21
−19
−17
−15
δ18O-H2O (‰)